Biomedicine & Pharmacotherapy 140 (2021) 111728

Contents lists available at ScienceDirect

Biomedicine & Pharmacotherapy

journal homepage: www.elsevier.com/locate/biopha

Original article

Antiproliferative and antimetastatic characterization of an *exo*-heterocyclic androstane derivative against human breast cancer cell lines

Ágnes E. Kulmány [a], Éva Frank [b], Dóra Kovács [b], Kerstin Kirisits [c], Georg Krupitza [c], Patrícia Neuperger [d], Róbert Alföldi [e], László G. Puskás [d,e], Gábor J. Szebeni [d,f], István Zupkó [a,*]

[a] Institute of Pharmacodynamics and Biopharmacy, University of Szeged, Szeged, Hungary
[b] Department of Organic Chemistry, University of Szeged, Szeged, Hungary
[c] Department of Pathology, Medical University of Vienna, Vienna, Austria
[d] Laboratory of Functional Genomics, Institute of Genetics, Eötvös Loránd Research Network Biological Research Centre, Szeged, Hungary
[e] Avidin Ltd., Szeged, Hungary
[f] Department of Physiology, Anatomy and Neuroscience, Faculty of Science and Informatics, University of Szeged, Szeged, Hungary

ARTICLE INFO

Keywords:
Androstane
Antiproliferative
Antimetastatic
Single-cell drug effect
Breast cancer

ABSTRACT

Cancer in general, and specifically gynaecological neoplasms, represents a major public health issue worldwide. Based on the effect of sex hormones on breast tumorigenesis and prognosis, as well as on the development of breast cancer metastases, modification of the steroid skeleton is a hotspot of research for novel anticancer agents. Numerous recent studies support that minor modifications of the androstane skeleton yield potent antiproliferative and antimetastatic drug candidates. The aim of the present study was to assess the antitumor and antimetastatic properties, as well as the mechanism of action of a D-ring-modified *exo*-heterocyclic androstadiene derivative named 17APAD. The test compound was found to be highly selective towards human breast cancer-derived cell lines (MCF-7, T47D, MDA-MB-361, MDA-MB-231) compared to non-cancerous fibroblast cells (NIH/3T3), and exerted superior effect compared to the clinically applied reference drug cisplatin. Changes in MCF-7- and MDA-MB-231 cell morphology and membrane integrity induced by the test substance were assessed by fluorescent double staining. Cell cycle disturbances were analyzed by flow cytometry, and concentration-dependent alterations were detected on breast cancer cell lines. Mitochondrial apoptosis induced by the test compound was demonstrated by JC-1 staining. Inhibitory effects on metastasis formation, including the inhibition of migration, invasion and intravasation were investigated in 2D and 3D models. Significant anti-migratory and anti-invasive effects on MCF-7 and MDA-MB-231 cells were detected after 24 h exposure in 2D wound healing and Boyden-chamber assays. The anti-intravasative properties of 17APAD were evident after 4 h of incubation in a co-culture 3D circular chemorepellent-induced defects (CCID) assay, and the level of inhibition at concentrations $\geq$2 μM was comparable to that exerted by the focal adhesion kinase inhibitor defactinib. Single cell mass cytometry revealed that chemosensitive subpopulations of MDA-MB-231 cells engaged to apoptosis were less positive for EGFR, CD274, and CD326, while the percentage of cells positive for GLUT1, MCT4, Pan-Keratin, CD66(a,c,e), Galectin-3 and TMEM45A increased in response to 17APAD treatment. Finally, the novel androstane analogue 17APAD had an outstanding inhibitory effect on tumour growth in the 4T1 orthotopic murine breast cancer model *in vivo* after 2 weeks of intraperitoneal administration. These findings support that substitution of the androsta-5,16-diene framework with a *N*-containing heterocyclic moiety at C17 position yields a molecular entity rational to be considered for design and synthesis of novel, effective antitumor agents, and 17APAD is worth further investigation as a promising anticancer drug candidate.

1. Introduction

Cancer represents a significant public health burden and is the second leading cause of death worldwide. Based on the GLOBOCAN 2018 survey of population-based cancer registries, malignancies are the main cause of death before age 70 in developed countries. Collecting

* Corresponding author.
E-mail address: zupko.istvan@szte.hu (I. Zupkó).

https://doi.org/10.1016/j.biopha.2021.111728
Received 11 March 2021; Received in revised form 6 May 2021; Accepted 11 May 2021
Available online 19 May 2021

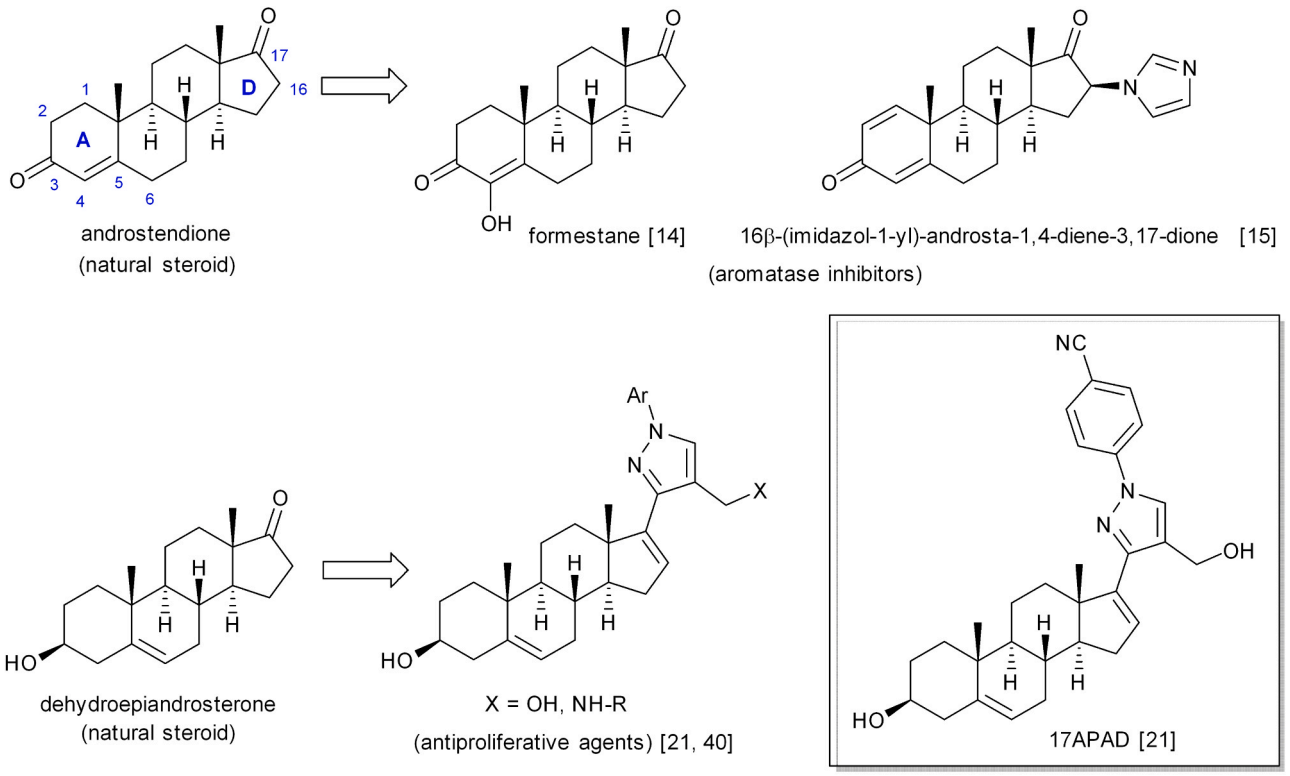

Fig. 1. Some representatives of anticancer agents derived from natural steroids and the chemical structure of 17APAD.

incidence and mortality data on 36 cancer types from 185 countries, this overview estimated 18.1 million new cancer cases and 9.6 million cancer-related deaths in 2018. Although trends and distributions greatly differ from region to region, a significant rise in both the incidence and mortality is expected over the next two decades. Among gynaecological malignancies, breast cancer is associated with the highest incidence and mortality. Among females, it is the most commonly diagnosed tumour type (11.6%, with 2.1 million new cases) and the leading cause of cancer death (6.6%, with ~627,000 deaths) worldwide [1–4].

Several risk factors responsible for the development of breast cancer have been identified, including genetic predisposition (*e.g.* mutations of *BRCA1* and *BRCA2* genes), aging, higher overall estrogen exposure (nulliparity, late age at first childbirth, long-term hormone therapy), high breast density, a history of atypical hyperplasia, and lifestyle effects (Western-style diet, obesity, alcohol consumption) [5,6]. Hereditary (mutation of BRCA2 and androgen receptor genes), hormonal (*e.g.* hyperprolactinaemia, long-term treatment with anti-androgens and estrogens) or environmental (external radiation) risk factors and aging can lead to breast cancer in men as well, but its incidence is less than 1% of all cancers in men and less than 1% of all breast cancers [7,8]. Population-based breast cancer screening services are of crucial importance for early diagnosis, which is key to improve the chance for successful therapy [9,10]. However, while early-stage breast cancer is often curable, breast tumours detected in an advanced stage still have generally poor prognosis, thus novel treatment options are eagerly awaited.

Due to the well-known effects of estrogens and androgens on cell proliferation and growth of hormone-dependent tumour tissues, one of the prominent areas of pharmacological research focuses on chemical modifications of the steroid skeleton to develop potent antitumor compounds. Structures of nuclear steroid receptors and their agonist and antagonist ligands are highly conserved, so minor modifications of the endogenous ligands at the appropriate positions, such as in the A- or D-ring, can yield compounds with completely novel biological activities [11,12]. Several recent studies have reported on modified androstane derivatives that exert potent enzyme-inhibitory, antiproliferative or antimetastatic activities in breast cancer cell lines [13]. Enzymes that modulate steroid biosynthesis and metabolism (*e.g.* aromatase, 17β-hydroxysteroid dehydrogenase, *etc.*) play a crucial role in maintaining physiological hormone levels. Thus, the inhibition of these enzyme proteins significantly reduces the level of endogenous estrogens and androgens, which is essential in the therapy of hormone-sensitive tumours. Aromatase is one of the most important enzymes involved in steroid hormone biosynthesis, mediating the conversion of androgens into estrogens (*e.g.* the biosynthesis of estrone from androstenedione or estradiol from testosterone). Therefore, aromatase inhibitors of steroidal (formestane and exemestane) or non-steroidal types are an integral part of the available treatment strategies for estrogen-dependent breast cancer, as well as of the research for novel drug candidates (Fig. 1). One of these research areas focuses on the functionalization of androstenedione at various positions [14]. As a part of these efforts, Bansal et al. have reported on novel 16-imidazolyl substituted steroidal compounds, of which two, 16β-(imidazol-1-yl)-4-androstene-3,17-dione and 16β-(imidazol-1-yl)-androsta-1,4-diene-3,17-dione were demonstrated to exert a potent aromatase inhibitory activity with IC_{50} values of 0.18 μM and 0.168 μM, respectively [15] (Fig. 1). Another important enzyme of steroid biosynthesis is 17β-hydroxysteroid dehydrogenase (17β-HSD), whose subtypes catalyze numerous steroidogenic reactions and inactivation of steroid hormones. Types 1 and 7 of 17β-HSD convert estrone into estradiol, thus the inhibition of these enzyme subtypes can hinder the proliferation of estrogen-dependent tumour tissues. Bellavance et al. and Wang et al. have reported on 17β-substituted 4-methyl-4-*aza*-5*R*-androstane derivatives, namely INH1 and INH7, which remarkably decrease the reduction of estrone into estradiol *via* the inhibition of 17β-HSD1 and/or 17β-HSD7 with IC_{50} values ranging from 189 nM to 451 nM. In addition, both INH1 and INH7 were demonstrated to suppress cell proliferation in MCF-7 and T47D breast cancer cells lines. Their antiproliferative activity is mediated by cell cycle arrest in the G0/G1 phase *via* the inhibition of cyclin D1 and the activation of p21 proteins, as well as by modulating the levels of anti-apoptotic and

pro-apoptotic proteins (Bcl-2, Bik), manifesting as a measurable shrinkage of malignant masses in an MCF-7 xenograft tumour model [16,17].

Similarly, A- or D-ring modified androstane analogues were also reported to exert pronounced antiproliferative activity in different cancer cell lines, especially against breast cancer cells. Scherbakov et al. synthesized numerous pyrimidine- and dihydrotriazine-derivatives of steroids in the androstane and estrane series, and the most promising compounds were demonstrated to have a growth inhibitory potential (IC_{50} values ranging from 7.4 to 21.6 μM) on MCF-7 and MDA-MB-231 cell lines. Additionally, the lead molecule bearing a dihydrotriazine moiety at the C16 position was shown to be selective towards MCF-7 breast cancer cells, with 50% inhibition of the activity of the estrogen receptor α without exerting any estrogen agonist activities [18]. Ajdukovic and co-workers described the antiproliferative and proapoptotic properties of some novel A-ring-modified 17α-picolyl and 17(*E*)-picolinylidene androstane derivatives, demonstrated in 6 different human malignant cell lines (MCF-7, MDA-MB-231, PC-3, HeLa, A549, HT-29), showing preferable selectivity towards the MCF-7 and PC-3 cells [19].

As the majority of cancer-related deaths are caused by metastases, modern drug research is partly directed towards the development of antimetastatic compounds. Wang et al. reported on E-salignone amide derivatives synthesized from epiandrosterone and androsterone, exerting favourable antimigratory effects and inhibiting the EGF-induced invasion of MDA-MB-231 cells [20].

In a previous study, we characterized a novel group of 17-(4′-formyl) pyrazolylandrosta-5,16-dienes – structurally related to dehydroepiandrosterone – that exerted promising antiproliferative activity on adherent breast cancer cell lines, and had a potent inhibitory effect on $C_{17,20}$-lyase, a rat testicular enzyme [21] (Fig. 1). The aims of the present study were to explore tumour selectivity, mechanism of action and antimetastatic properties of a potential drug candidate of this series (17APAD).

2. Materials and methods

2.1. Chemicals and cell cultures

3β-Hydroxy-17-[1′-(4"-cyanophenyl)-4′-hydroxymethyl-1′*H*-pyrazol-3′-yl]androsta-5,16-diene (17APAD; Fig. 1) was synthesized as reported previously [21]. MCF-7, MDA-MB-231 and NIH/3T3 cell lines were purchased from ECACC (European Collection of Cell Cultures, Salisbury, UK), and the 4T1 cell line was acquired from ATCC (American Tissue Culture Collection, Manassas, Virginia, USA). A telomerase immortalized human lymphatic endothelial cell line (T1S1/iLEC) was established and characterized by the Medical University of Vienna (Vienna, Austria). MCF-7, MDA-MB-231 and NIH/3T3 cells were maintained in Eagle's Minimum Essential Medium (EMEM) supplemented with 10% fetal bovine serum (FBS), 1% non-essential amino acid solution and 1% penicillin, streptomycin and amphotericine B mixture at 37 °C, in humidified atmosphere containing 5% carbon dioxide (CO_2). iLECs, owning to their special requirements, were grown in EGM-2 MV medium (EGM-2 MV BulletKit, Lonza), under the same conditions. The 4T1 mouse breast cancer cells were cultured in RPMI medium complemented with 10% FBS, 1% non-essential amino acid mixture and 1% antibiotic solution, and were kept in a CO_2 incubator at 37 °C. Passage numbers of all cells used in the experiments were less than 25. All media, supplements, chemicals and kits used for the experiments and cell culturing, were obtained from Sigma-Aldrich Ltd. (Budapest, Hungary) unless otherwise specified.

2.2. Antiproliferative (MTT) and tumour selectivity assays

Promising antiproliferative properties of 17APAD on four adherent breast cancer cell lines with different receptor expression profiles have been published earlier [21]. For a more detailed exploration of these experimental data, the standard antiproliferative assay was repeated on non-cancerous fibroblast cells (NIH/3T3) under the same conditions [22]. NIH/3T3 cells were seeded onto 96-well plates in a density of 5000 cells/well, and were treated with increasing concentrations of the drug candidate (0.1–30 μM). After 72 h of incubation, 3-(4,5-dimethylthiazol-2-yl)-2,5-diphenyltetrazolium bromide solution (MTT, 5 mg/mL in phosphate buffer) was added. After 4 h of exposure, the supernatants were gently removed and the precipitated blue formazan crystals were dissolved in 100 μL dimethyl sulfoxide (DMSO). Absorbance values were recorded by a microplate reader (Stat Fax 2100, Awareness Technologies, Westport, CT, USA) at 545 nm, and data of normalized six-point dose-response curves were fitted by the GraphPad Prism 5.0 software (GraphPad Software, San Diego, CA, USA). Untreated cells were used as a control, and a stock solution of 17APAD was prepared with DMSO. The maximum concentration of DMSO (0.3%) exerted no substantial effect on the proliferation of the cells we utilized.

2.3. Hoechst 33258–propidium iodide fluorescent double staining

To characterize the changes in cell morphology and cell membrane integrity after treatment with 17APAD, fluorescent double staining was carried out. MCF-7 cells were seeded onto 96-well plates in a density of 5000 cells/well, were incubated overnight in a CO_2 thermostat, and then were treated with different concentrations of 17APAD for 24 h. Next, the cells were stained by lipophilic Hoechst 33258 (5 μg/mL, HO) and hydrophilic propidium iodide (3 μg/mL, PI) for 1 h under the same circumstances described for cell culturing above. After refreshing the medium on the samples, at least 10 images/condition were taken by a Nikon Eclipse TS100 fluorescence microscope (Nikon Instruments Europe, Amstelveen, The Netherlands) equipped with appropriate optical blocks for Hoechst 33258 (excitation: 360/40 nm bandpass filter, emission: 460/50 nm bandpass filter and 400 nm dichromatic mirror) and propidium iodide (excitation: 500/20 nm bandpass filter, emission: 520 nm longpass filter and 515 nm dichromatic mirror), and the images were analyzed by the QCapture Pro software (QImaging, Surrey, British Columbia, Canada). Nuclei were counted (300–900 cells/image, depending on the applied concentration of 17APAD), and the ratios of different cell populations were expressed.

2.4. Apoptosis assay

To further characterize the proapoptotic property of 17APAD, Annexin V-Alexa 488– propidium iodide (PI) combined fluorescent staining was performed with flow cytometry detection as described previously [23]. MCF-7 and MDA-MB-231 cells were grown on 24-well cell culture plates (80,000 cells/well) and were treated with increasing concentrations (1, 2, 4 and 8 μM) of 17APAD. After 24 h of incubation, the cells were washed with phosphate buffered saline (PBS), harvested by trypsin and pooled with collected supernatants. After centrifugation (1400 rpm for 5 min at room temperature), the cells were resuspended in Annexin V binding buffer (ABB; 0.01 M HEPES, 0.14 M NaCl and 2.5 mM $CaCl_2$, pH = 7.4) and were stained with Annexin V-Alexa 488 (LifeTechnologies, Waltham, MA, USA) for 15 min in dark, at room temperature. PI (10 μg/mL) in ABB was added directly before acquisition to dilute (5x) Annexin V-Alexa 488. For each sample 10,000 events were recorded by a FACSCalibur cytofluorimeter (BD Biosciences, San Jose, CA, USA), and the data were analyzed by the CellQuest™ software (Becton Dickinson, New Jersey, USA).

2.5. Cell cycle analysis

In order to gain a more detailed insight into the effects of 17APAD on cell cycle in the tested breast cancer cell lines, cell cycle analysis was accomplished as described previously [24]. Briefly, estrogen and progesterone receptor positive MCF-7 and triple negative MDA-MB-231 cell lines were seeded onto 24-well plates (80,000 cells/well). The samples

were treated with increasing concentrations of 17APAD for 48 h or 72 h, washed with PBS and collected after trypsinization. Cells were pooled with the collected supernatants and PBS from washing, and were centrifuged at 1400 rpm for 5 min at room temperature. Pellets were resuspended and stained by our DNA staining solution (10 μg/mL PI, 0.1% Triton-X, 10 μg/mL RNase A, and 0.1% sodium citrate dissolved in PBS) for 30 min in dark, at room temperature. Detection of DNA content from at least 20,000 cells/sample were carried out by a FACSCalibur flow cytometer, and the obtained data were analyzed by the Kaluza Analysis Software (Beckman Coulter, Brea, California, USA). Untreated cells were considered as control. Hypodiploid subG1 phases were regarded as evidence of a late apoptotic event.

2.6. Mitochondrial membrane potential assay (JC-1 staining)

To elucidate the mechanism of action of 17APAD, the origin of induced apoptosis was examined by the JC-1 assay as described previously [25]. JC-1 is a voltage-sensitive dye which can accumulate and aggregate in mitochondria, and emits red light when the mitochondrial membrane potential is physiological. In contrast, when the mitochondrial membrane potential is disrupted, the accumulation of JC-1 is reduced, leading to a shift from red to green fluorescence. MCF-7 and MDA-MB-231 human breast cancer cells and 4T1 mouse mammary tumour cells were maintained and harvested under standard conditions described above, and the cell suspension was seeded onto 24-well plates in the density of 10^5 cells/well. After the administration of 17APAD and incubation for 12 h, the cells were washed with PBS, trypsinized and collected, pooled with the corresponding supernatant and centrifuged at 2000 rpm for 5 min. Next, pellets were re-suspended in JC-1 (Chemodex, St. Gallen, Switzerland) solution containing 5 μg/mL dye, and were incubated for 15 min at 37 °C. Finally, the red and green fluorescence signals of cells were detected on FL2 (585/42 nm) – FL1 (530/30 nm) channels by the FACSCalibur flow cytometer. In each analysis, 10,000 events were recorded and data analysis was carried out by the CellQuestTM software (Becton Dickinson, New Jersey, USA).

2.7. Wound-healing assay

The MCF-7 cell suspension was prepared in EMEM medium supplemented with 2% FBS, 1% non-essential amino acid solution and 1% penicillin, streptomycin and amphotericine B mixture, and it was implanted into special silicone inserts (Ibidi GmbH, Gräfelfing, Germany) placed on 12-well plates, in a density of 20,000 cells/well. After an overnight incubation, the inserts were gently removed, the cells were wash with PBS, and were treated with low concentrations of 17APAD. The size of cell-free areas were determined by the ImageJ software (National Institutes of Health, Bethesda, Maryland, USA), based on images taken at 0, 24 and 48 h post-treatment.

2.8. Boyden-chamber assay

Special Boyden-chambers were applied to identify treatment effects on cancer cells' invasion capacity. These inserts contain two medium-filled compartments separated by a PET membrane with a pore size of 8 μm and a thin layer of matrigel basement matrix as an *in vitro* model of the extracellular environment. Suspension of highly invasive MDA-MB-231 cells, prepared in serum-free EMEM medium supplemented with sub-antiproliferative concentrations of 17APAD, were nested into the upper chamber, onto prehydrated membrane, while the EMEM medium supplemented with 10% FBS was used as chemoattractant in the lower chamber. After 24 h of incubation, the supernatants and non-invading cells were removed cautiously with a cotton swab, and the membranes were washed with PBS twice. Samples were fixed in ice cold 96% ethanol, and were stained by 1% crystal violet dye for 30 min in dark, at room temperature. Images (at least 3 per insert) were taken by a Nikon Eclipse TS100 microscope, and invading cells were counted and compared to untreated control samples.

Table 1
Antibodies used for mass cytometry.

Catalogue number	Supplier	Target	Metal tag
3170009B	Fluidigm	EGFR	^{170}Er
3156026B	Fluidigm	CD274 (PD-L1)	^{156}Gd
3141006B	Fluidigm	CD326 (EpCam)	^{141}Pr
MAB1418	R&D Systems	GLUT1	^{154}Sm
sc-376140	Santa Cruz Biotech.	MCT4	^{171}Yb
3162027A	Fluidigm	Pan-Keratin	^{162}Dy
3149018B	Fluidigm	CD66-a,c,e	^{149}Sm
3153026B	Fluidigm	Galectin-3 (Gal-3)	^{153}Eu
orb357227	Biorbyt	TMEM45A	^{169}TM

2.9. Circular chemorepellent-induced defects assay (CCID)

As a 3D model of intravasation, a circular chemorepellent-induced defects assay was performed in co-culture to assess the inhibitory activity of 17APAD on metastasis formation. Tumour spheroids were prepared from MCF-7 cells, and iLEC human lymphendotelial cells were grown to almost 100% confluency on 24-well plates under cell culturing conditions. Cancer cells were harvested by trypsin and resuspended in EMEM medium supplemented with methylcellulose solution (in a final concentration of 0.3%), and were seeded onto U-bottom 96-well plates in a density of 3000 cells/well. The plates were centrifuged (1500 rpm, 15 min, room temperature) and the samples were grown for approximately 3 days to form spheroids. Upon starting the analysis, the iLEC monolayer was stained by CellTracker Green dye (ThermoFisher Scientific, Waltham, Massachusetts, USA) for 1 h at 37 °C. Next, the fluorescent labelled endothelial barrier was washed by PBS and preincubated with 17APAD for 20 min. Spheroids with appropriate size and shape were selected, washed and preincubated with 17APAD for 20 min as well. After pretreatment, tumour spheroids were placed on the lymphendotelial cell monolayer and were incubated with 17APAD for 4 h in CO_2 atmosphere at 37 °C. Spheroids and iLEC monolayer treated with complete medium supplemented with 0.1% DMSO were used as controls. To assess lymphendothelial defects resembling intravasation, images of at least 12 spheroids per condition from three biologically independent samples were taken by a fluorescent Axiovert microscope (Zeiss GmbH, Jena, Germany). CCID areas and the size of spheroids were evaluated by the Zen Little 2012 software (Zeiss GmbH, Jena, Germany).

2.10. Single cell mass cytometry

Single cell mass cytometry was carried out as described previously [24]. Briefly, MDA-MB-231 cells were plated (4×10^5 cells/well in 6-well plates) in 3 mL EMEM medium containing 8 μM 17APAD, and were incubated for 72 h. Control samples were left untreated. Three separate experiments were performed at three different time points. After treatment for antibody staining, three technical replicate wells were pooled. The cells were washed with PBS and were liberated by Accutase (Corning Life Sciences, Ny, USA), centrifuged (5 min, 350g), re-suspended in PBS and counted using a Bürker chamber and trypan blue viability dye (Sigma-Aldrich) before being processed for mass cytometry staining. Viability of the cells was determined by cisplatin staining (5 μM 195Pt, Fluidigm, CA, USA) for 3 min on ice in 300 μL PBS. Samples were diluted with 1500 μL Maxpar Cell Staining Buffer (MCSB, Fluidigm) and were centrifuged at 350g for 5 min. Non-specific binding of the antibodies was avoided by incubating the cells with TruStain FcX (Biolegend, CA, USA), 2.5 μL in 50 μL MCSB (PBS containing blocking proteins) for 10 min. Cells were centrifuged (350g, 5 min) and suspended in 50 μL MCSB, and the resultant antibody mix (Table 1) was added to 50 μL of fresh master pool of antibodies. The following antibodies were conjugated with metal tags in-house: anti-CA9, anti-GLUT1, anti-MCT4 and anti-TMEM45A, using a Maxpar

metal labelling kit and strictly following to the instructions of the manufacturer (Fluidigm). All the antibodies were titrated prior to the experiment in order to determine their optimal level of dilution.

After incubating the samples for 60 min at 4 °C, the antibodies were washed by 2 mL MCSB and centrifuged at 300g for 5 min, twice. The pellet was suspended in the residual volume. The cells were fixed in 1.6% formaldehyde (freshly diluted from 16% Pierce formaldehyde with PBS, Thermo Fisher Scientific) and incubated at room temperature for 10 min. Next, the cells were centrifuged at 800g for 5 min. Cell-ID DNA intercalator (^{191}Ir/^{193}Ir, Fluidigm) was added in 1:1000 dilution in Maxpar Fix and Perm buffer (Fluidigm) and the sample was incubated overnight at 4 °C. The sample was centrifuged at 800g for 5 min, then it was washed with 2 mL MCSB and centrifuged again at 800g for 5 min. The cells were suspended in 1 mL PBS (for WB injector) and were counted in a Bürker chamber after centrifugation. For the acquisition, the concentration of cells was set to 0.3×10^6/mL in a cell acquisition solution (CAS, Fluidigm) containing 10% EQ Calibration Beads (Fluidigm). The cells were filtered through a 30 μm gravity filter (Celltrics, Sysmex Partec, Japan) and were acquired freshly. Mass cytometry data were analyzed by the Cytobank software (Beckman Coulter). Cell debris and aggregates were excluded, and singlets were determined by manual gating using the ^{191}Ir and ^{193}Ir DNA intercalators. Next, untreated single cells and cells with hampered viability (^{195}Pt+) were manually gated positive for the investigated markers. The t-SNE (t-distributed stochastic neighbour embedding) analysis (iterations = 1000, perplexity = 30, theta = 0.5), was carried out on 1.5×10^4 events of untreated singlets *versus* treated single cells with drug-sensitivity (^{195}Pt+). The before-after plots based on pooled data of three biological replicates demonstrate the percentage of cells positive for a given marker in untreated control samples compared to the percentage of MDA-MB-231 cells sensitive to 8 μM 17APAD.

2.11. In vivo mouse breast cancer model

To examine the antineoplastic properties of 17APAD *in vivo*, an orthotopic mouse breast cancer model was used according to the methodology utilized in a previous study [26]. The experiments were executed in accordance with the EU rules (2010/63/EU) on animal experimentation and ethics. The experimental protocol was approved by the responsible governmental agency (National Food Chain Safety Office) in concordance with the ethical clearance No. XXIX./128/2013.

Two groups (test *vs.* control, 7 animals per group) of BALB/c mice (weighing 18–26 g) were housed in a sterile, IVC cage system protected by a Hepa filter, at ambient temperature of 25 °C. On day 1 of the experiment, 120,000 4T1 breast carcinoma cells, maintained, harvested and re-suspended in FCS-free RPMI medium, were injected into the orthotopic mammary pad of each animal. On day 12, the animals were randomized into test *vs.* control groups. The mean tumour size was approximately equal in each group (mean values between 22 and 25 mm^3). The test group was treated with 25 mg/kg 17APAD dissolved in a mixture of DMSO/Solutol HS 15/saline (1:3:10) once daily, intraperitoneally, five times a week for 2 weeks. The control group was treated with the vehicle mixture. Tumour size and body mass were measured daily (d^2 *x* D *x* 0.5, where d and D are minor and major tumour diameters, respectively). After the treatment period, the animals were sacrificed, primary tumour tissues were removed and their weights were measured.

2.12. Statistical analysis

The GraphPad Prism version 5.01 software was used for statistical analysis. Statistical significance was estimated by one-way analysis of variance (ANOVA) followed by the Dunnett post-test. All presented results are means ± SEM of at least three replicates. *, ** and *** indicate $P < 0.05$, $P < 0.01$ and $P < 0.001$ compared to control, respectively.

Table 2
Calculated IC_{50} values and tumour selectivity (TS) indices for 17APAD and cisplatin (CIS), assessed on human breast cancer cell lines and a non-cancerous fibroblast cell line (NIH/3T3).

Cell line	IC_{50} (μM)	TS_{17APAD}	IC_{50} CIS (μM)	TS_{CIS}
MCF-7	1.40*	0.368	5.78#	2.143
T47D	1.20*	0.316	9.78#	3.626
MDA-MB-361	1.60*	0.473	3.74#	1.387
MDA-MB-231	1.80*	0.421	19.13#	7.093
NIH/3T3	3.75	–	2.70	–

Note: * and # indicate literature data [21,27].

3. Results

3.1. 17APAD selectively inhibited cell proliferation of breast cancer cell lines

Remarkable growth inhibitory effect of our test compound 17APAD on human breast cancer cell lines was demonstrated previously, indicating that 17APAD is more potent than the clinically applied control cisplatin [21]. Tumour selectivity (TS) investigated in our study is expressed as the ratio of the IC_{50} values for 17APAD and cisplatin control (CIS) on breast cancer and non-cancerous fibroblast cells (Table 2). TS indices for 17APAD and cisplatin were ≤0.473 and ≥1.387, respectively, indicating a higher tumour selectivity of 17APAD in human breast cancer cell lines compared to cisplatin.

3.2. 17APAD induced programmed cell death via the activation of mitochondrial pathway of apoptosis in breast cancer cells

Changes in cell morphology and cell membrane integrity of breast cancer cell were visualized by fluorescent nuclei staining using Hoechst 33258 and propidium iodide dyes after 24 h exposure to 2 or 4 μM 17APAD. Fluorescence microscopy analysis revealed early apoptotic cells with bright blue fluorescence owing to the penetration of Hoechst 33258 dye, while secondary necrotic nuclei eradiated red fluorescence owing to the penetration of propidium iodide. Significant increments were observed in the number of MCF-7 cells showing early signs of apoptosis or the natural outcome of the complete apoptotic program (Fig. 2).

While the microscopic detection of fluorescent staining has limitations regarding cell number count and the separation of early *vs.* late apoptotic and necrotic cells, flow cytometry allows of detecting a higher number of events and a more precise distinction of different cell populations. In both types of human breast cancer cells (MCF-7 and MDA-MB-231), 17APAD induced a concentration-dependent activation of phosphatidylserine exposure, which can be regarded as an indicator of late apoptotic cells (late apoptosis: AnnV+/PI+) without the presence of a massive necrotic cell population (necrosis: AnnV-/PI+) (Fig. 3).

To elucidate the possible mitochondrial origin of apoptosis, a JC-1 assay was performed. Green fluorescence of the monomer form of JC-1 in cells with depolarized mitochondrial membrane were recorded by a flow cytometer, and its quantitative analysis showed significant, concentration-dependent increments in the proportion of cells with damaged mitochondrial function in all cell lines 12 h post-treatment with 17APAD (Fig. 4).

3.3. 17APAD induced cell-cycle arrest

Cell cycle disturbances induced by 17APAD were assessed by cell cycle analysis. A concentration-dependent rise of hypodiploid subG1 cell populations, regarded as a marker of induced apoptosis, were observed in both cell lines (MCF-7, MDA-MB-231) (Fig. 5). Compared to untreated control, >12-fold and >8-fold changes were detected in the MCF-7 and MDA-MB-231 cell lines, respectively. Moreover, in the MCF-7 cell line, considerable elevations in the proportion of G2/M phases at the expense

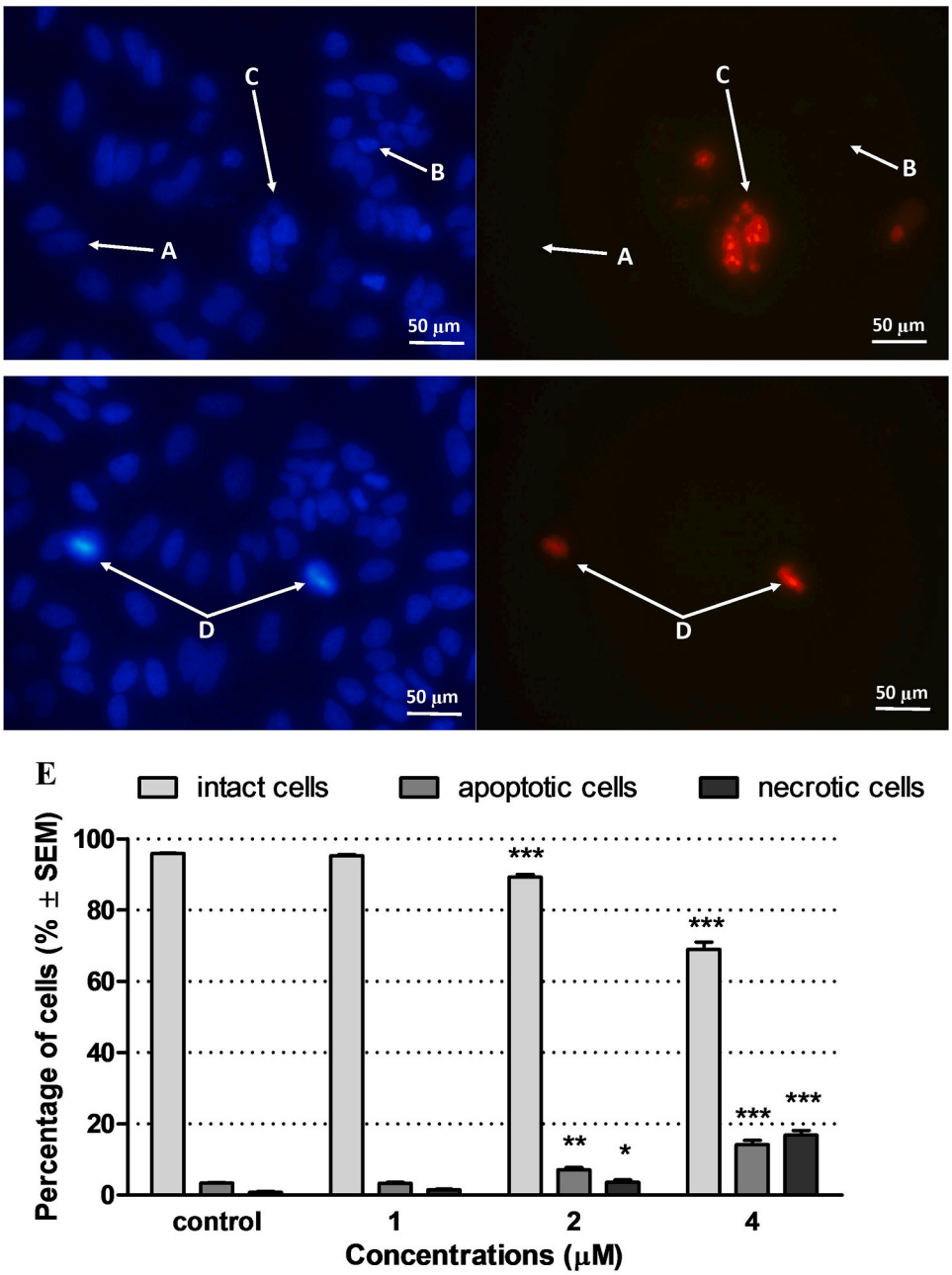

Fig. 2. 17APAD induced the accumulation of apoptotic and secondary necrotic cell populations. Intact (A), early apoptotic (B), late apoptotic (C) and necrotic (D) MCF-7 nuclei stained by Hoechst 33258 (blue fluorescence, left panels) and propidium iodide (red fluorescence, right panels) after 24 h of treatment with 2 μM 17APAD were analyzed by fluorescent microscopy at 400× magnification. The percentages of intact, apoptotic and necrotic cell populations were calculated (E). Data represent mean ± SEM. *, ** and *** indicate significant differences between 17APAD-treated and untreated control samples at $P < 0.05$, $P < 0.01$ and $P < 0.001$, respectively (For interpretation of the references to colour in this figure legend, the reader is referred to the web version of this article).

of the G1 phase were detected after 48 h of treatment (results of analysis 72 h post-treatment are presented in Supplementary Material). Under the same conditions, the highly invasive, triple negative breast cancer cell line MDA-MB-231 showed signs of G2/M cell cycle arrest and a modest reduction of the proportion of cells in the G1 phase 48 h after 17APAD treatment. These changes were even more pronounced 72 h post-treatment (Fig. 6).

3.4. 17APAD reduced migration, invasiveness and intravasation of breast cancer cells

To determine the anti-migratory effect of 17APAD, changes in the size of cell-free areas were measured at 0, 24 h and 48 h post-treatment using samples with reduced serum-containing medium. A reduction of cell-free gaps, produced by special silicon inserts, was demonstrated by image analysis of wound closure. A significant decrease in wound healing was detected at 24 h and 48 h post-treatment even when sub-antiproliferative concentrations of 17APAD (*i.e.* <10% of the antiproliferative threshold value in the 72 h MTT assay) were applied, indicating a remarkable inhibition of tumour cell migration in cell lines treated with our test compound (Fig. 7).

Besides cell migration, cellular invasion and infiltration of the surrounding tissues are crucial to the development of tumour metastases. Therefore, we supplemented our wound healing assay of cellular migration with a special Boyden chamber assay as the extracellular environment of primary tumours, to study cellular invasion. For this purpose, because of non-invasive characteristic of MCF-7 cells, the highly invasive MDA-MB-231 breast cancer cell line was selected. In this experimental system, a noticeable decline of the invasive potential of MDA-MB-231 cells was observed as soon as 24 h post-treatment upon applying sub-antiproliferative concentrations (0.1 μM and 0.3 μM) of 17APAD (Fig. 8).

Available 2D assay data indicate a promising antimetastatic property of 17APAD, thus a co-culture circular chemorepellent-induced defects

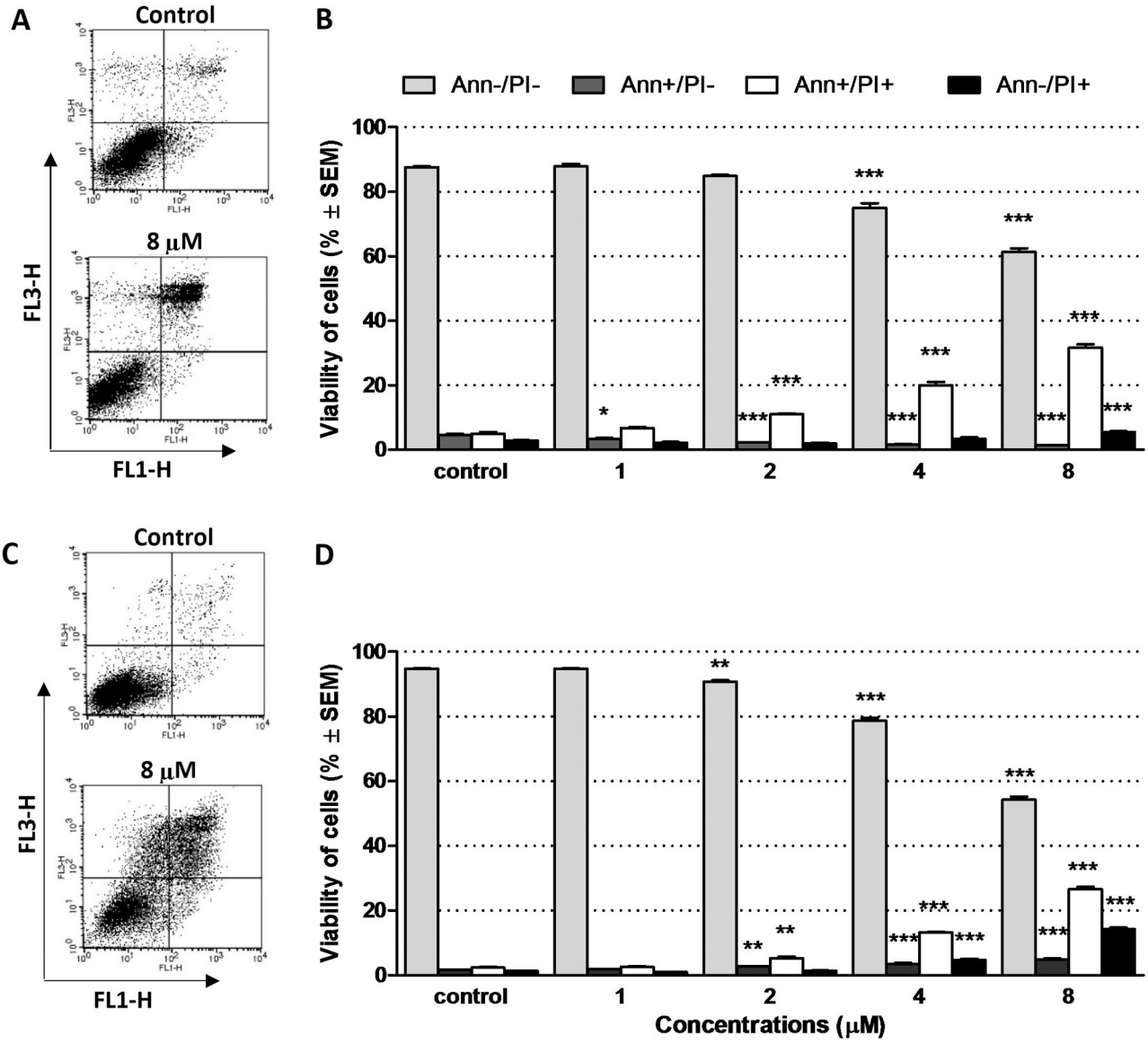

Fig. 3. 17APAD exerted a proapoptotic effect both in MCF-7 and MDA-MB-231 cells. Representative dot-plot figures and percentages of viable (AnnV-/PI-), early apoptotic (AnnV+/PI-), late apoptotic (AnnV+/PI/), and necrotic (AnnV-/PI+) populations of MCF-7 (A–B) and MDA-MB-231 (C–D) cells. Cells were treated with 17APAD for 24 h or were left untreated for control. A concentration-dependent increase in the rate of late apoptotic and necrotic fractions were observed in both cell lines, while the ratio of early apoptotic cells was elevated in the MDA-MB-231 and was reduced in the MCF-7 cell line. Data are presented as mean ± SEM. *, ** and *** indicate $P < 0.05$, $P < 0.01$ and $P < 0.001$, respectively, compared to control.

assay was carried out to demonstrate antimetastatic activity in a 3D model of intravasation. After 4 h of treatment with 17APAD at a concentration of ≥2 μM, a remarkable and concentration-dependent decrease in the size of cell-free areas were observed on the confluent lymphendothelial cell monolayer underneath the tumour spheroids (Fig. 9). At a concentration of 4 μM, 17APAD reduced the areas of cell-free gaps by approximately 25%, which is comparable to the inhibitory effect of defactinib, a potent focal adhesion kinase (FAK) inhibitor agent currently investigated in clinical trials, and used as a positive control in our experiments.

3.5. 17APAD induced changes in the expression level of 9 specific carcinoma markers in triple-negative breast cancer cells

In order to characterize the chemosensitive subpopulations of MDA-MB-231 cells, nine carcinoma markers were investigated at single cell resolution following treatment with 8 μM 17APAD. The multidimensional analysis, the visualization of t-distributed stochastic neighbour embedding (viSNE), revealed the clonal heterogeneity of single-cell effects induced by 17APAD on the MDA-MB-231 cell line. The area of viSNE plots unequivocally discriminated between untreated control and 17APAD-sensitive cells. The colour changes of single cells detected upon treatment are proportional to the expression level of the specific carcinoma markers defining various subpopulations of MDA-MB-231 cells (Fig. 10A). After 72 h of incubation the percentage of cells positive for EGFR, CD274 (PD-L1), and CD326 (EpCAM) showed a gradual decrease within the drug-sensitive population, as determined by manual gating. On the contrary, the cells engaged to apoptosis showed an increased expression of GLUT1, MCT4, Pan-Keratin, CD66 (a,c,e), Galectin-3 and TMEM45A (Fig. 10B).

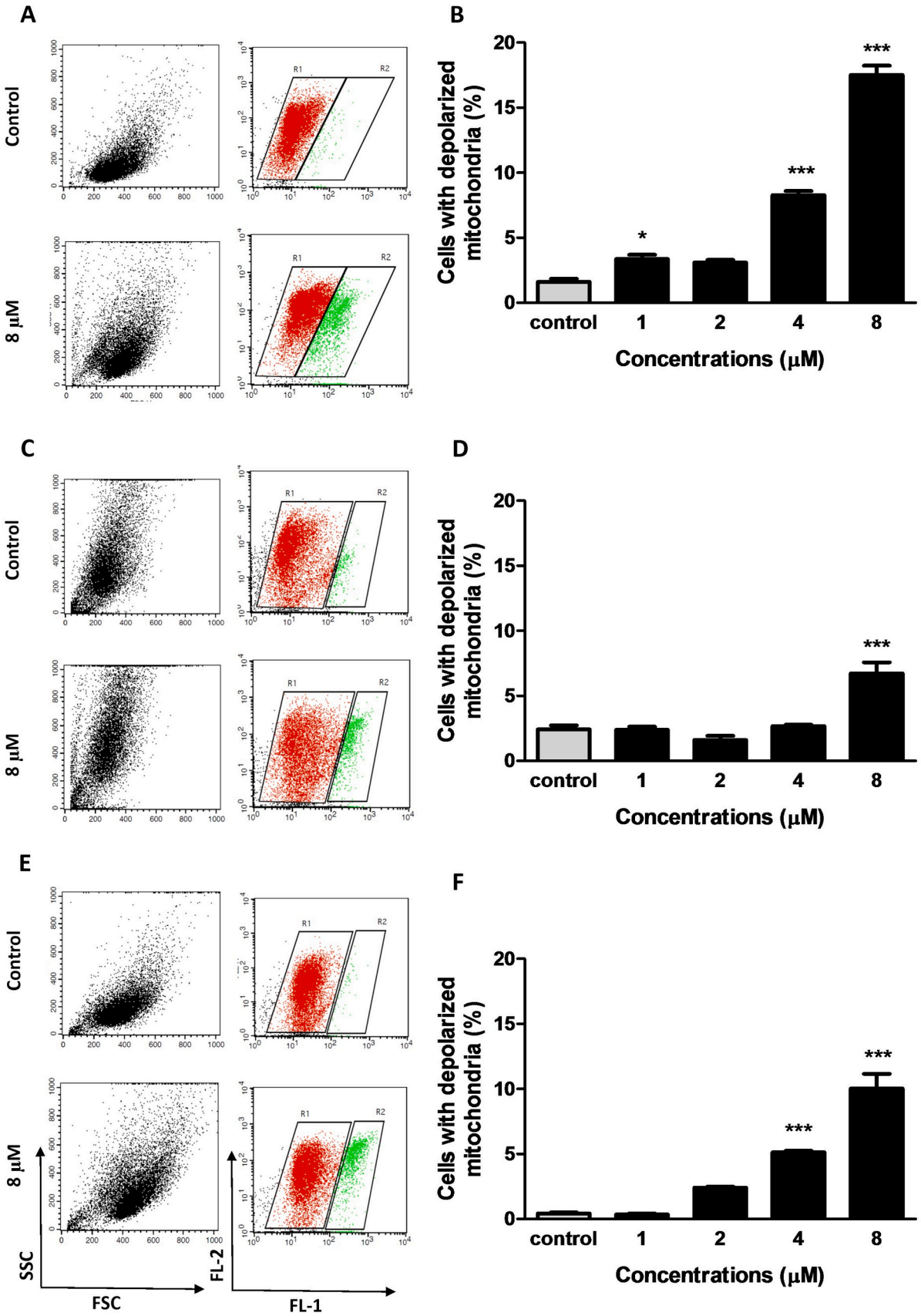

Fig. 4. 17APAD induced a loss of mitochondrial membrane integrity in breast cancer cell lines. Proportions of MCF-7 (B), MDA-MB-231 (D) and 4T1 (F) cells with depolarized mitochondrial membrane 12 h post-treatment and their representative dot-plot graphs showing treatment effects upon treatment with the highest concentration of 17APAD (A, C, E) are presented compared to untreated control. Values are mean ± SEM. * and *** indicate $P < 0.05$ and $P < 0.001$, respectively, compared to control.

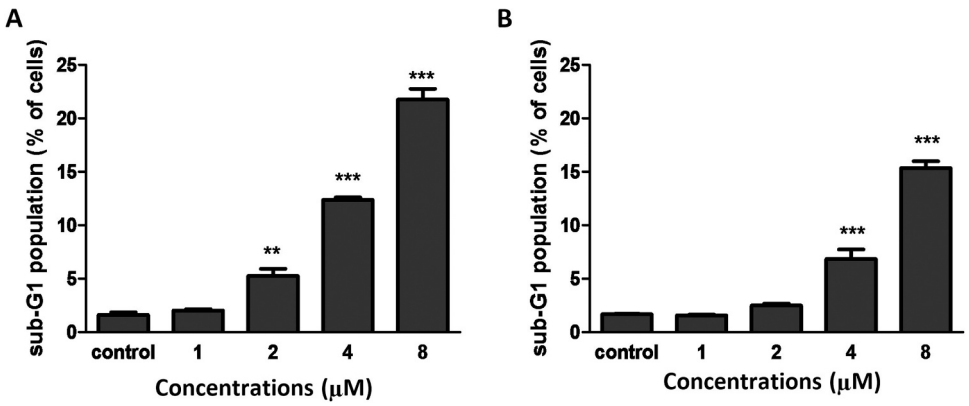

Fig. 5. 17APAD (1, 2, 4 or 8 μM) induced significant and concentration-dependent elevations in the proportion of apoptotic sub-G1 cell populations in the MCF-7 (A) and MDA-MB-231 cell lines (B) 48 h post-treatment. Untreated cells were used as control. Data are presented as mean ± SEM. ** and *** indicate $P < 0.01$ and $P < 0.001$, respectively, compared to control.

3.6. Treatment of 17APAD highly reduced the tumour growth rate in 4T1 mouse breast cancer model in vivo

A 4T1 orthotopic mouse breast cancer model, accepted as an excellent *in vivo* model of breast cancer development and metastasis [28,29] was used to test the antimetastatic properties of 17APAD. The test group of animals was administered 17APAD intraperitoneally, for 2 weeks at a dose of 25 mg/kg. As compared to the untreated control group, the mean tumour weight was significantly reduced in the treated group, from 971.8 mg to 504.1 mg. Besides, tumour growth curves indicate that the progression of tumour allografts significantly slowed down after the fourth day of the treatment compared to the controls (Fig. 11). Importantly, no serious or life-threatening side effects were observed in the experimental group.

4. Discussion

Molecules with a steroidal skeleton are ubiquitously distributed in nature, and include fungal sterols, phytosterols and steroid hormones in animals and humans. These natural products are responsible for a wide range of essential physiological functions, such as the maintenance of cellular structure and communication within the organism. Since the primary functions of sexual steroids are strongly associated with tissue development and proliferation, these mediators are also involved in the progression of several malignant disorders of such as breast, ovarian, prostate and colorectal cancers [30].

Several recent studies have demonstrated that modifying of the structure of endogenous human sexual steroids (estrogens and androgens) at the appropriate positions, especially at the A- and/or D-rings (including the incorporation of new substituents like heterocyclic rings) may yield effective and potent semi-synthetic or synthetic derivatives with a wide spectrum of biological activities, while preserving the favourable pharmacological and pharmacokinetic properties of the steroid frame (such as the rigid skeleton and lipophilicity) [13]. Some of these molecular products are already an integral part of oncotherapy (abiraterone) or are currently undergoing clinical trials (galeterone) based on experimental evidence supporting their promising *in vivo* activities. Many steroid analogues applied as therapeutic agents share a common characteristic: they are generally substituted at the C17 position with a proton donor or acceptor *exo*-heterocyclic ring that alters the molecule's binding affinity to its receptors, leading to fundamentally altered biological properties compared to the parent compound [31–34].

Nuclear hormone receptors, such as estrogen or androgen receptors have highly conserved protein structures, characterized by a ligand-binding region consisting of 12 helices. The hydrogen bonds between the 3-keto group and the side chains at residues Q711 and R752, as well as between the 17β-OH group and the side chains at N705 and T877, or moieties mimicking these bonds play an essential role in the activation of the androgen receptor [35,36]. Upon designing effective, novel anticancer drug candidates with a sterane skeleton, all these structural requirements should be considered in order to avoid undesirable side effects of hormonal origin. Based on our previous research and literature data, D-ring substituted androstane analogues containing the heterocyclic ring pyrazole were designed and synthesized. Favourable antiproliferative properties of this molecular family have been reported on breast cancer cell lines, thus the most promising compound, 17APAD was selected for further investigation in the current study. Determining its mechanism of action would facilitate the design of potent anticancer and antimetastatic steroid analogues [21,27,37].

The IC_{50} values of our drug candidate 17APAD did not exceed 2 μM on breast cancer cell lines, while cisplatin, used as a positive control, showed the same level of inhibitory effect in the concentration range between 3.74 and 19.13 μM. Furthermore, the tumour selectivity index of 17APAD was found to range from 0.316 to 0.473, while the same index for cisplatin exceeded 1 (1.39–7.09), supporting a higher selectivity of 17APAD in breast cancer cell lines. These findings are in agreement with literature data for other structurally related compounds, including abiraterone [21,38,39].

Regarding the mechanism of action of any promising antineoplastic compounds, destroying tumour cells by inducing programmed cell death is a crucial touchstone of effectiveness. The early steps of this process can be specified by morphological changes at the cell level, including chromatin condensation in early apoptotic cells and loss of membrane integrity in necrotic and secondary necrotic cells. To visualize these phenomena, Hoechst–propidium iodide fluorescent DNA staining was applied on MCF-7 cells after 24 h incubation with different concentrations of 17APAD. Significant increases in the proportion of apoptotic and necrotic cell populations were observed in MCF-7 samples at concentrations $\geq$2 μM, indicating a potent proapoptotic characteristic of 17APAD. Additionally, annexin V-Alexa488/propidium iodide fluorescent labelling was carried out using flow cytometry. A remarkable elevation of the proportion of late apoptotic cells, and a significant but less prominent increase in the proportion of necrotic cell populations were observed in both the MCF-7 and MDA-MB-231 human mammary carcinoma cell lines after 24 h incubation with the androstadiene analogue 17APAD.

To further elaborate the mechanism of action of 17APAD, cell cycle analysis was carried out by flow cytometry on these two cell lines (MCF-7, MDA-MB-231). In case of the MCF-7 samples, a considerable elevation in the proportion of cells in the G2/M phase at the expense of the G1 phase was revealed. The highly invasive, triple negative breast cancer cell line MDA-MB-231 seemed to be less sensitive, however, signs of the same cell cycle distributions were detected at 48 h after 17APAD

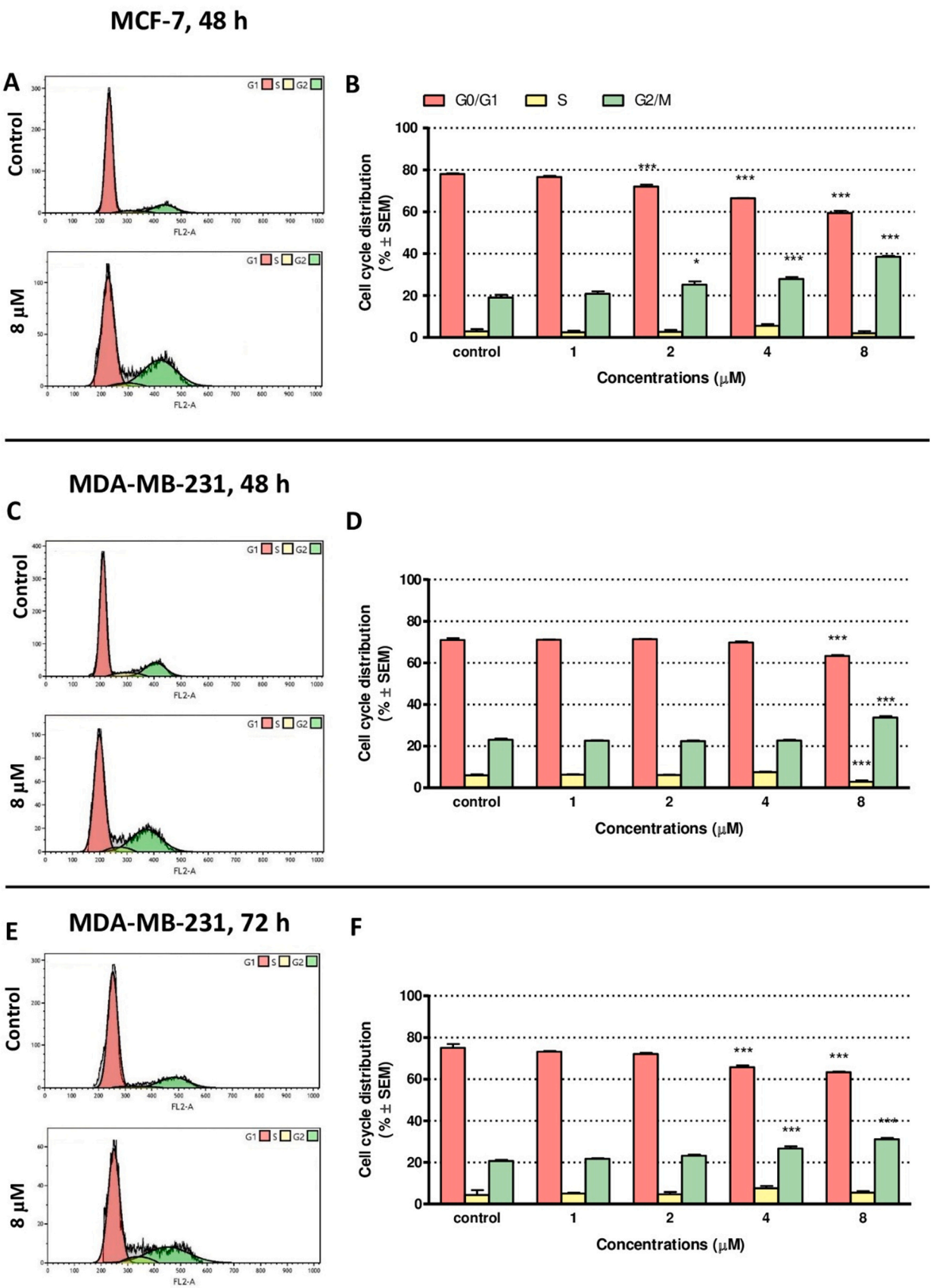

Fig. 6. 17APAD induced cell cycle disturbances in MCF-7 (A, B) and MDA-MB-231 (C–F) cells, as detected 48 h (A–D) and 72 h (E, F) post-treatment. A considerable elevation in the ratio of cells in the G2/M phase and a reduction in the proportion of cells in G0/G1 phase were evident by cell cycle analysis. Data are presented as mean ± SEM. *, ** and *** indicate $P < 0.05$, $P < 0.01$ and $P < 0.001$, respectively, compared to control.

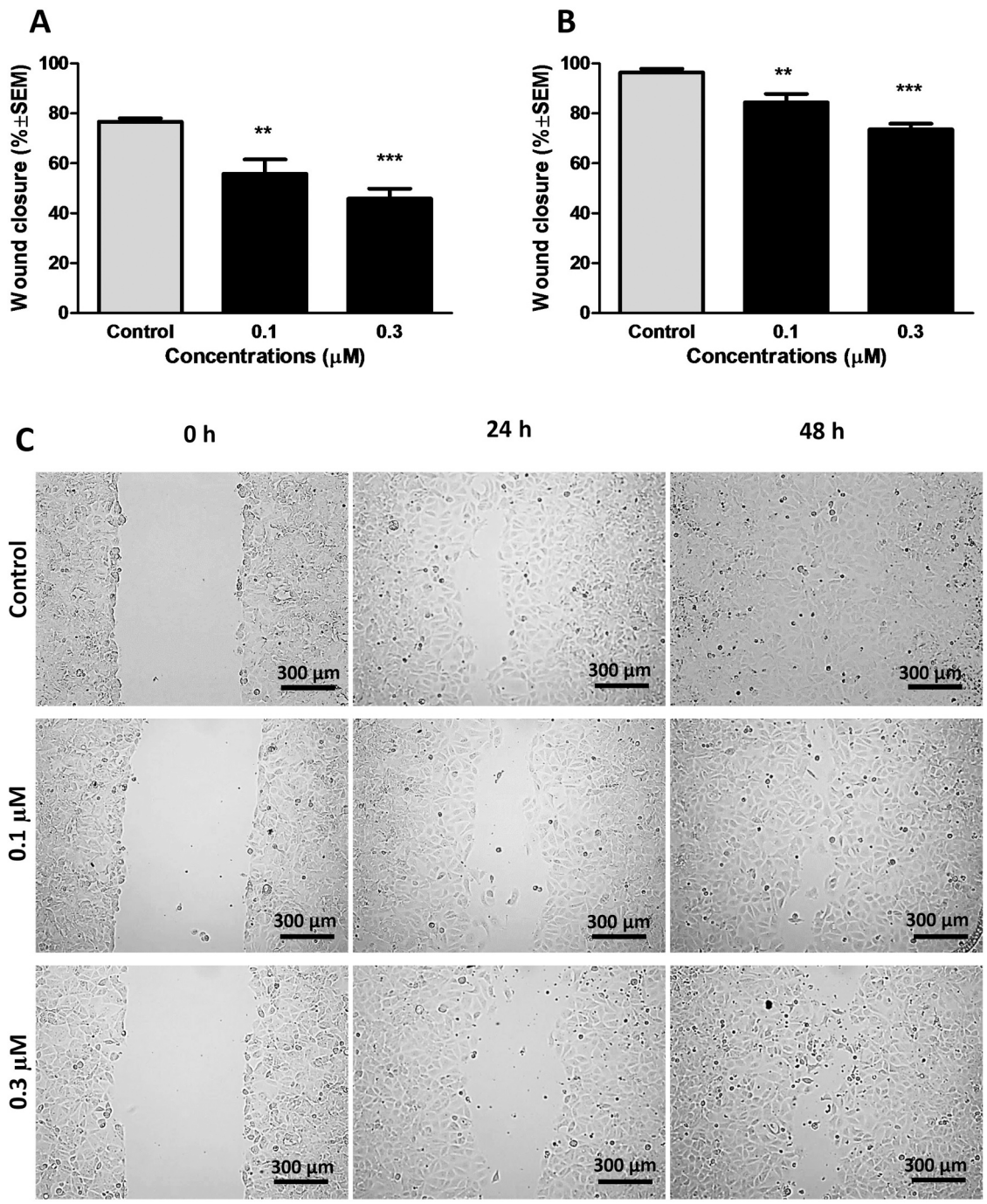

Fig. 7. 17APAD reduced/inhibited migration of breast cancer cells. Quantified rates of wound closure were significantly diminished in the presence of 17APAD. Graphs indicate the percentage of cell-free areas at 24 h (A) and 48 h (B) post-treatment in the MCF-7 cell line compared to control. Representative images of reduced wound healing at 0, 24 and 48 h post-treatment (C). Data are presented as mean ± SEM. ** and *** indicate $P < 0.01$ and $P < 0.001$, respectively, compared to control.

treatment, and these alterations became even more pronounced at 72 h post-treatment. This finding is in line with recent studies indicating that D-ring-modified androstane derivatives typically require 48 h of incubation to induce cell cycle anomalies [27,37]. Furthermore, the proportion of the hypodiploid subG1 fraction, regarded as the apoptotic population, increased in a concentration-dependent manner in both cell lines, supporting the proapoptotic property of 17APAD.

In a previous study, Li et al. reported on the potent antiproliferative and apoptosis-inducing features of an agent showing a high degree of structural similarity to 17APAD (Fig. 1). This compound, 17β-(1-phenyl-4-((ethylamino)methyl)-3-pyrazolyl)androst-5,16-dienes-3β-ol], has been demonstrated to exert pronounced growth inhibitory activity in 293 T (human kidney), A549 (lung carcinoma), HeLa (cervical epitheloid carcinoma) and MCF-7 (breast cancer) cell lines with IC_{50} values ranging from 0.53 to 7.39 μM. In addition, this androstane derivative was reported to induce nuclear condensation and appearance of apoptotic bodies in HeLa cells, visualized by Hoechst 33342 staining. Finally, it was reported to induce significant elevations of the apoptotic cell population using annexin V-FICT/PI staining and increase of the S phase proportion demonstrated by cell cycle analysis [40].

The morphological alterations specific to apoptosis are attributable to the cascades of biochemical interaction elicited by intrinsic or

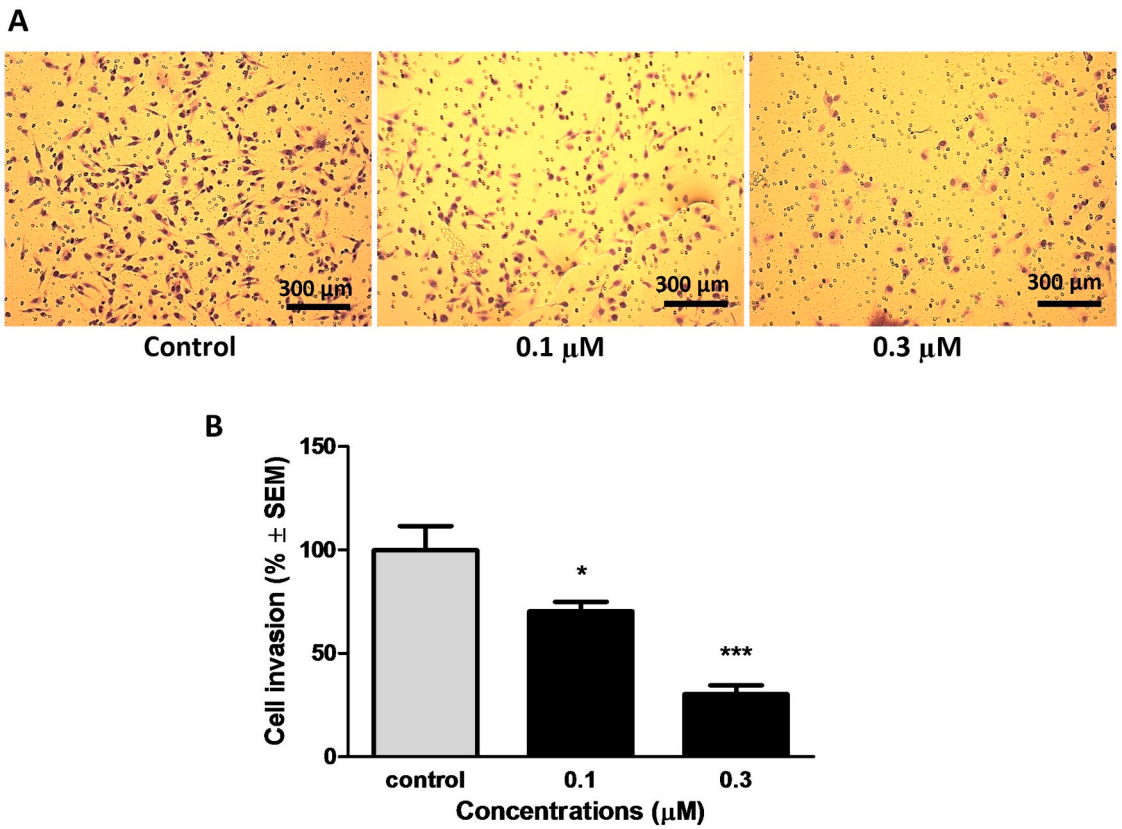

Fig. 8. 17APAD reduced the invasiveness of triple-negative breast cancer cells (MDA-MD-231). The anti-invasive potential of the test substance is demonstrated by representative images (A), and it is expressed by the percentage of invading cells in the Boyden chamber containing different concentrations of 17APAD using EMEM medium supplemented with 10% FBS as chemoattractant for MDA-MB-231 cells (B). Data are presented as mean ± SEM. * and *** indicate $P < 0.05$ and $P < 0.001$, respectively, compared to untreated control samples.

extrinsic initiation. Voltage-sensitive JC-1 staining indicated an impairment of mitochondrial membrane potential after 12 h of 17APAD treatment, corroborating that our test substance activates the intrinsic signal transduction mechanisms of apoptosis in human (MCF-7, MDA-MB-231) and murine (4T1) breast cancer cell lines.

It is generally accepted that the majority of deaths from solid tumors are caused by metastases, thus, the identification of drug-modifiable targets involved in the development and growth of metastases, and research for novel drug candidates capable to interfere with metastasis formation are eagerly required to reduce cancer mortality [41]. The role of sexual steroidal hormones in the process of metastasis formation is incompletely understood and is currently investigated. Regarding the highly invasive, triple negative breast cancer cell lines (MDA-MB-231 and MDA-MB-453), Giovannelli et al. have reported that androgens promote tumour invasiveness *via* the AR/Src/PI3-K complex, so progression may be reduced by antiandrogen administration [42–45]. The first steps of the metastatic cascade are migration and invasion of cancer cells through the basement membrane to reach the extracellular matrix and neighbouring tissues. In our study 17APAD significantly hindered the migration of MCF-7 cells after 24 h of exposure, and a remarkable, >20% difference in wound-closure rate of control and treated samples was detected at 48 h after adding 300 nM of 17APAD to the MCF-7 samples in a wound healing assay. Regarding the MDA-MB-231 cell line, the number of invasive tumour cells greatly decreased after 24 h of treatment with sub-antiproliferative, nanomolar concentrations (100 nM and 300 nM) of 17APAD.

However, cell motility alone is not sufficient for metastasis formation: migrating cells need to enter the circulatory system *via* lymphatic or blood vessels. Intravasation necessarily includes the interaction between cancer cells and the endothelial barrier, resulting in gap formation *via* different pathways [46]. As a 3D, co-culture model of the interactions between tumour cells and the endothelial monolayer, we implemented a circular chemorepellent-induced defects assay. The size of cell free-areas on the iLEC monolayer under MCF-7 tumour spheroids decreased by 30% after 4 h treatment with 17APAD at a concentration of 8 µM. This level of inhibition was comparable to that induced by defactinib, a potent focal adhesion kinase inhibitor currently investigated in clinical trials [47,48].

Targeting cell surface markers such as EGFR, CD274 or CD326, associated with the malignant characteristic and poor prognosis of solid tumours, is reported to enhance the chemosensitivity of tumour cells [49–51]. In agreement with these previous findings, 17APAD-sensitive subpopulations of MDA-MB-231 cells showed decreased expression of EGFR, CD274, and CD326 in our study. Besides, perturbation of the mitochondrial membrane potential induced by 17APAD, leading to oxidative stress in MDA-MB-231 cells was also shown. In line with the literature, we have found the metabolic reprogramming of cells may induce GLUT1 and MCT4 expression [52,53]. Increased expression of these regulators of breast cancer cell survival support glycolytic metabolism and lactate secretion as compensatory mechanisms getting activated upon oxidative stress [54,55]. Increased GLUT1 expression has also been reported in association with increased chemosensitivity in triple negative breast cancer cell lines [56]. Increased expression of Pan-Keratins on cell surface detected in our study (the clone C11 antibody detects keratins: 4, 5, 6, 8, 10, 13 and 18) can also be regarded as markers for increased sensitivity to host defence mechanisms, as Pan-Keratins are receptors for clearance by phagocytic cells [57]. In contrast, the carcinoembryonic antigen-related cell adhesion molecules (CEACAM) recognized by the antibody used in our study (CD66a = CEACAM1, CD66c = CEACAM6, CD66e = CEACAM5) are carcinoma

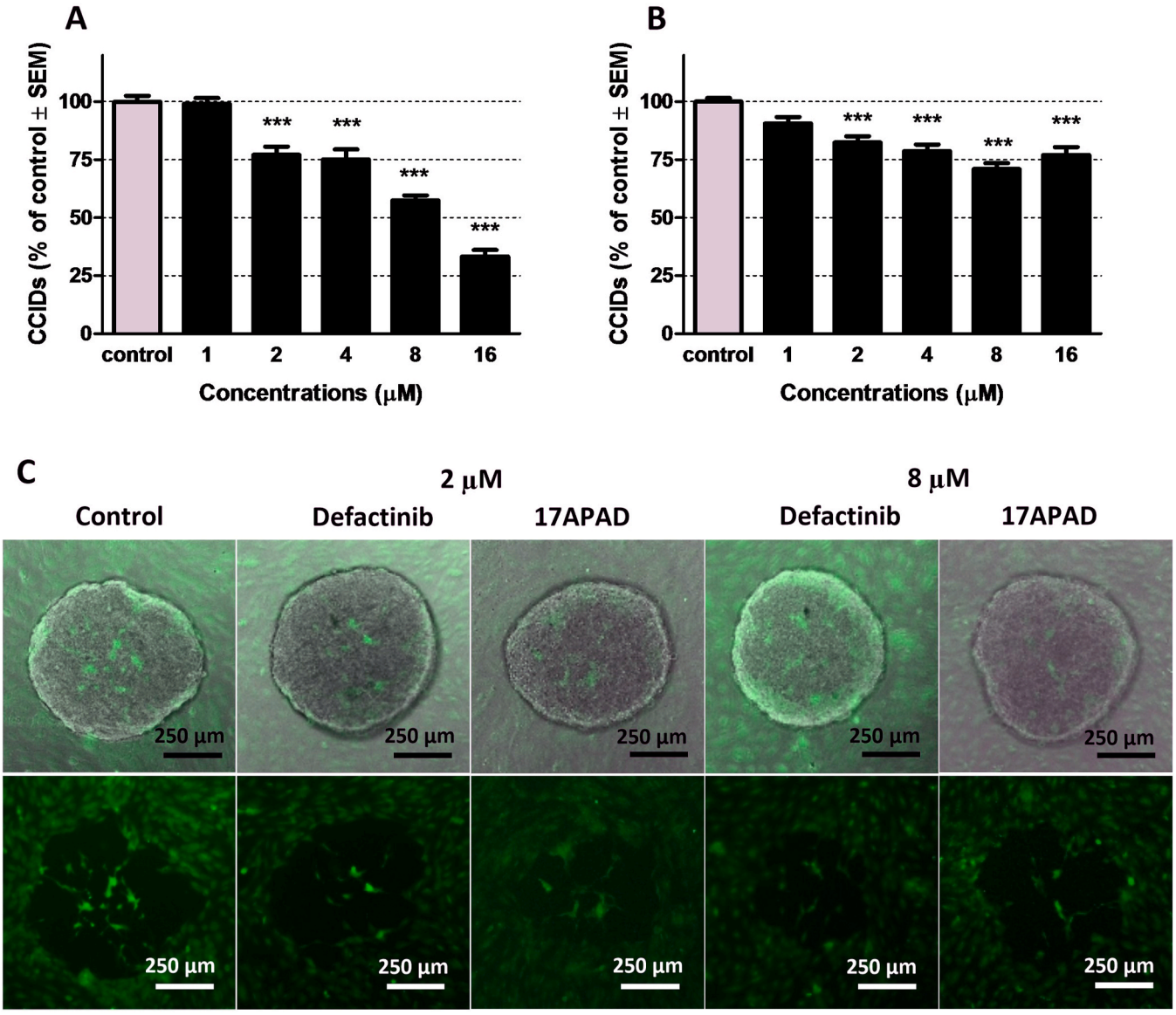

Fig. 9. 17APAD hindered gap formation underneath breast cancer spheroids. The decrease in the size of cell-free areas was comparable to that induced by a potent focal adhesion kinase (FAK) inhibitor defactinib used as a positive control. Reduction of the size of cell-free areas induced by defactinib (A) and 17APAD (B) after 4 h treatment on MCF-7/iLEC model, and representative images of cancer spheroids (upper panel in phase contrast microscopy) and beneath cytotracker-stained endothelial monolayer (lower panel fluorescence microscopy of the same microscopical frame) are presented (C). Data represent mean ± SEM. *** indicates $P < 0.001$ compared to the untreated control.

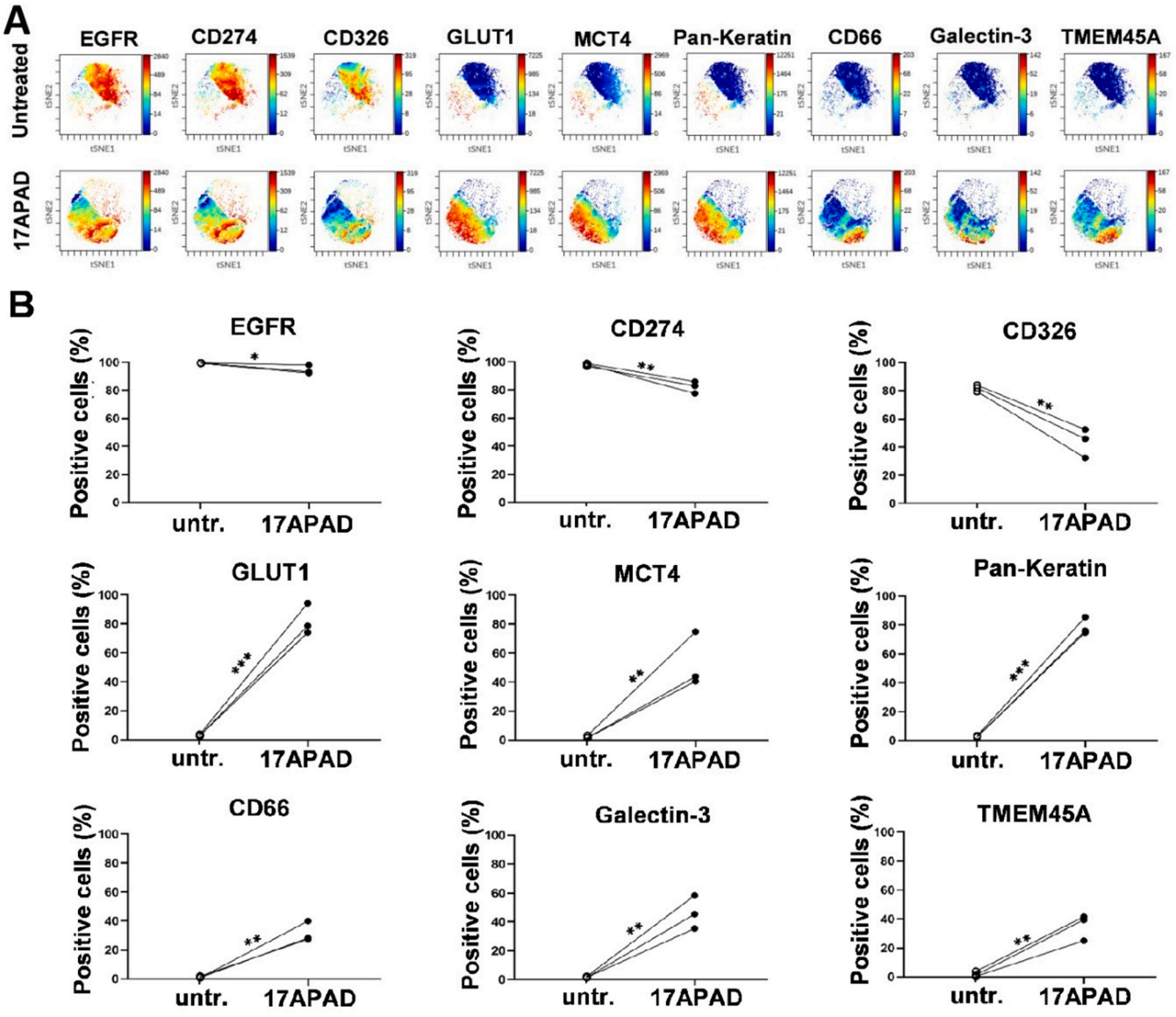

Fig. 10. Representative multidimensional visualization of 9 carcinoma marker proteins in the MDA-MB-231 cell line treated with 8 μM 17APAD and evaluated at single cell resolution 72 h post-treatment (A). Within the chemosensitive cell population, 17APAD reduced the percentage of cells positive for EGFR, CD274 and CD326, and increased the percentage of cells positive for GLUT1, MCT4, Pan-Keratin, CD66(a,c,e), Galectin-3, TMEM-45A (B). *, ** and *** indicate $P < 0.05$, $P < 0.01$ and $P < 0.001$, respectively, compared to control.

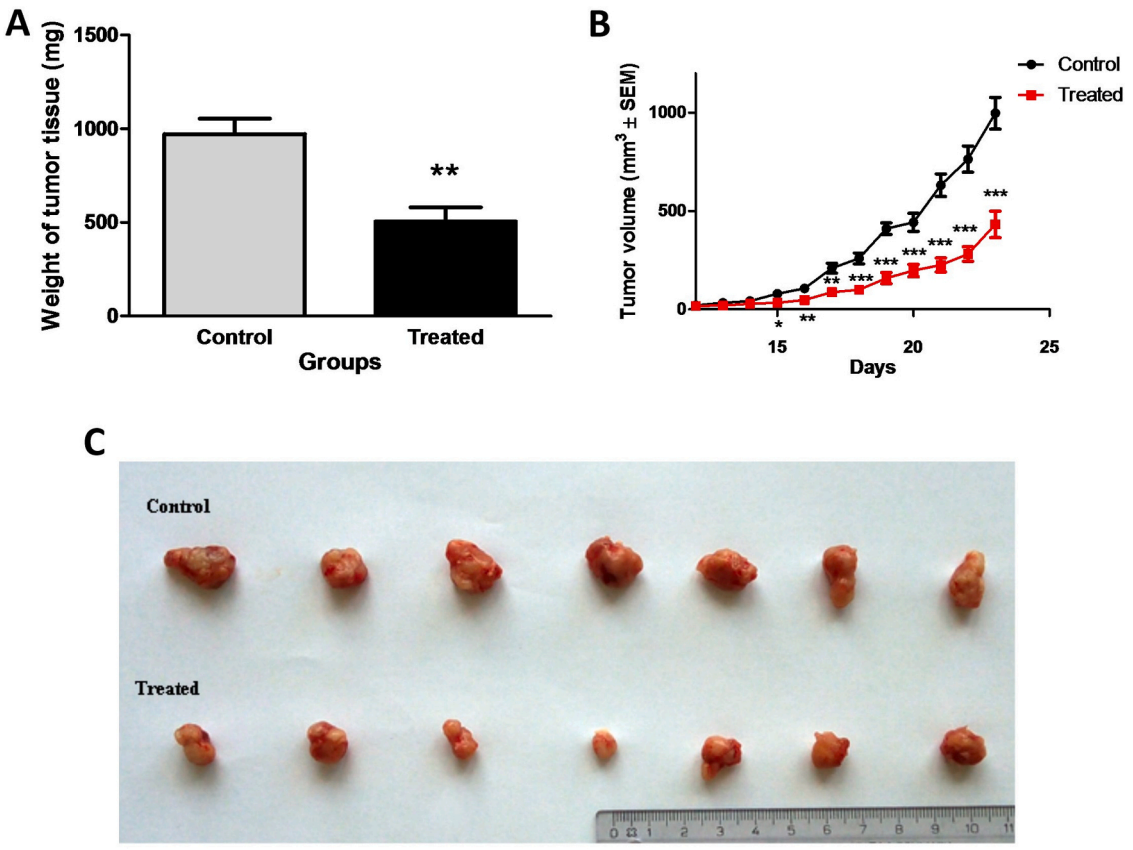

Fig. 11. Tumour growth rate significantly decreased after 17APAD treatment compared to the control group. The mean weight of isolated tumour tissues (n = 7) surgically removed after two weeks of intraperitoneal treatment with 17APAD significantly differed between the control and the experimental group (A). Tumour growth curves (B) and representative images of primary tumour tissues (C) demonstrate a considerable growth inhibitory effect of 17APAD in vivo. Data represent mean ± SEM. *, * * and *** indicate $P < 0.05$, $P < 0.01$ and $P < 0.001$, respectively, compared to control.

markers used in routine diagnostics, and are involved in cancer progression, angiogenesis and the development of metastasis [58]. Interestingly, the cells positive for CD66(a,c,e) overlapped with the population of cells positive for TMEM45A. The increase of both Galectin-3 and TMEM45A detected in a subpopulation of MDA-MB-231 cells have previously been reported to be responsible for chemoresistance and cancer cell survival under hypoxic conditions [59,60].

Finally, to determine whether the favourable antitumor properties of the *exo*-heterocyclic androstadiene derivative 17APAD demonstrated *in vitro* are also evident *in vivo*, a BALB/c mice model of 4T1 breast cancer was used. This orthotopic animal model mimics stage IV, highly invasive, triple-negative human breast cancer. After 2 weeks of intraperitoneal administration of 17APAD tumour growth rate was substantially reduced, without any serious side effects detected. Upon dissection, the mean weight of primary tumours was found to be reduced by approximately 50% compared to vehicle-treated controls.

In conclusion, our experimental data support the promising antiproliferative and antimetastatic effects of 3β-hydroxy-17-[1′-(4"-cyanophenyl)-4′-hydroxymethyl-1′*H*-pyrazol-3′-yl]androsta-5,16-diene (17APAD for short). Apoptosis-induction *via* activating the intrinsic pathway of programmed cell death accompanied by moderate tumour selectivity, as well as the potent anti-migratory, anti-invasive and anti-intravasative effects of the test substance have been identified as part of its mechanism of action. In light of these findings, 17APAD is worth further investigation as a potential drug candidate with antiproliferative and antimetastatic properties but besides *in vivo* testing on mice, further toxicological and pharmacokinetic characterization of this compound is necessary to provide a forecast of its potential biological, health and environmental impacts. Besides, our findings support that the substitution of the androsta-5,16-diene framework at C17 position with a *N*-containing heterocyclic moiety yields a molecular entity rational to be considered for design and synthesis of novel, effective antitumor agents.

Conflict of interest statement

The authors declare that they have no competing interests.

Acknowledgements

Financial supports provided by the Economic Development and Innovation Operative Program GINOP-2.3.2-15-2016-00012, GINOP-2.3.2-15-2016-00030 (BRC), the UNKP-19-3-SZTE-169 and UNKP-20-4-SZTE-324 New National Excellence Program, as well as grant 20391-3/2018/FEKUSTRAT of the Ministry of Human Capacities are highly appreciated. The authors thank Dora Bokor, PharmD, for proofreading the manuscript.

Appendix A. Supporting information

Supplementary data associated with this article can be found in the online version at doi:10.1016/j.biopha.2021.111728.

References

[1] F. Bray, J. Ferlay, I. Soerjomataram, R.L. Siegel, L.A. Torre, A. Jemal, Global cancer statistics 2018: GLOBOCAN estimates of incidence and mortality worldwide for 36 cancers in 185 countries, CA Cancer J. Clin. 68 (2018) 394–424, https://doi.org/10.3322/caac.21492.

[2] J. Ferlay, M. Colombet, I. Soerjomataram, T. Dyba, G. Randi, M. Bettio, A. Gavin, O. Visser, F. Bray, Cancer incidence and mortality patterns in Europe: estimates for

40 countries and 25 major cancers in 2018, Eur. J. Cancer 103 (2018) 356–387, https://doi.org/10.1016/j.ejca.2018.07.005.
[3] R.L. Siegel, K.D. Miller, A. Jemal, Cancer statistics, 2018, CA Cancer J. Clin. 68 (2018) 7–30, https://doi.org/10.3322/caac.21442.
[4] R.-M. Feng, Y.-N. Zong, S.-M. Cao, R.-H. Xu, Current cancer situation in China: good or bad news from the 2018 Global Cancer Statistics? Cancer Commun. 39 (2019) 22, https://doi.org/10.1186/s40880-019-0368-6.
[5] A. McTiernan, P. Porter, J.D. Potter, Breast cancer prevention in countries with diverse resources, Cancer 113 (2008) 2325–2330, https://doi.org/10.1002/cncr.23829.
[6] M.C. Mahoney, T. Bevers, E. Linos, W.C. Willett, Opportunities and strategies for breast cancer prevention through risk reduction, CA Cancer J. Clin. 58 (2008) 347–371, https://doi.org/10.3322/CA.2008.0016.
[7] A.G. Zygogianni, G. Kyrgias, C. Gennatas, A. Ilknur, V. Armonis, M. Tolia, C. Papaloukas, G. Pistevou, J. Kouvaris, V. Kouloulias, Male breast carcinoma: epidemiology, risk factors and current therapeutic approaches, Asian Pac. J. Cancer Prev. 13 (2012) 15–19, https://doi.org/10.7314/APJCP.2012.13.1.015.
[8] A.J. Abdelwahab Yousef, Male breast cancer: epidemiology and risk factors, Semin. Oncol. 44 (2017) 267–272, https://doi.org/10.1053/j.seminoncol.2017.11.002.
[9] N.J. Massat, A. Dibden, D. Parmar, J. Cuzick, P.D. Sasieni, S.W. Duffy, Impact of screening on breast cancer mortality: the UK Program 20 Years On, Cancer Epidemiol. Biomark. Prev. 25 (2016) 455–462, https://doi.org/10.1158/1055-9965.EPI-15-0803.
[10] M. Dahlui, S. Ramli, A.M. Bulgiba, Breast cancer prevention and control programs in Malaysia, Asian Pac. J. Cancer Prev. 12 (2011) 1631–1634.
[11] G.M. Anstead, K.E. Carlson, J.A. Katzenellenbogen, The estradiol pharmacophore: ligand structure-estrogen receptor binding affinity relationships and a model for the receptor binding site, Steroids 62 (1997) 268–303, https://doi.org/10.1016/S0039-128X(96)00242-5.
[12] A.G. Fragkaki, Y.S. Angelis, M. Koupparis, A. Tsantili-Kakoulidou, G. Kokotos, C. Georgakopoulos, Structural characteristics of anabolic androgenic steroids contributing to binding to the androgen receptor and to their anabolic and androgenic activities, Steroids 74 (2009) 172–197, https://doi.org/10.1016/j.steroids.2008.10.016.
[13] É. Frank, G. Schneider, Synthesis of sex hormone-derived modified steroids possessing antiproliferative activity, J. Steroid Biochem. Mol. Biol. 137 (2013) 301–315, https://doi.org/10.1016/j.jsbmb.2013.02.018.
[14] M.R. Yadav, M.A. Barmade, R.S. Tamboli, P.R. Murumkar, Developing steroidal aromatase inhibitors-an effective armament to win the battle against breast cancer, Eur. J. Med. Chem. 105 (2015) 1–38, https://doi.org/10.1016/j.ejmech.2015.09.038.
[15] R. Bansal, S. Guleria, S. Thota, S.L. Bodhankar, M.R. Patwardhan, C. Zimmer, R. W. Hartmann, A.L. Harvey, Design, synthesis and evaluation of novel 16-imidazolyl substituted steroidal derivatives possessing potent diversified pharmacological properties, Steroids 77 (2012) 621–629, https://doi.org/10.1016/j.steroids.2012.02.005.
[16] É. Bellavance, V. Luu-The, D. Poirier, Potent and selective steroidal inhibitors of 17β-hydroxysteroid dehydrogenase type 7, an enzyme that catalyzes the reduction of the key hormones estrone and dihydrotestosterone, J. Med. Chem. 52 (2009) 7488–7502, https://doi.org/10.1021/jm900921c.
[17] X. Wang, C. Gérard, J.-F. Thériault, D. Poirier, C.J. Doillon, S.-X. Lin, Synergistic control of sex hormones by 17β-HSD type 7: a novel target for estrogen-dependent breast cancer, J. Mol. Cell Biol. 7 (2015) 568–579, https://doi.org/10.1093/jmcb/mjv028.
[18] A.M. Scherbakov, A.V. Komkov, A.S. Komendantova, M.A. Yastrebova, O. E. Andreeva, V.Z. Shirinian, A. Hajra, I.V. Zavarzin, Y.A. Volkova, Steroidal pyrimidines and dihydrotriazines as novel classes of anticancer agents against hormone-dependent breast cancer cells, Front. Pharmacol. 8 (2017) 979, https://doi.org/10.3389/fphar.2017.00979.
[19] J.J. Ajduković, K.M. Penov Gaši, D.S. Jakimov, O.R. Klisurić, S.S. Jovanović-Šanta, M.N. Sakač, L.D. Aleksić, E.A. Djurendić, Synthesis, structural analysis and antitumor activity of novel 17α-picolyl and 17(*E*)-picolinylidene A-modified androstane derivatives, Bioorg. Med. Chem. 23 (2015) 1557–1568, https://doi.org/10.1016/j.bmc.2015.02.001.
[20] H.-L. Wang, N. Qin, J. Liu, M.-N. Jin, X. Zhang, M.-H. Jin, D. Kong, S.-D. Jiang, H.-Q. Duan, Synthesis and antimetastatic effects of *E*-salignone amide derivatives, Drug Dev. Res. 75 (2014) 76–87, https://doi.org/10.1002/ddr.21157.
[21] D. Kovács, J. Wölfling, N. Szabó, M. Szécsi, Z. Schelz, I. Zupkó, É. Frank, Synthesis of novel 17-(4′-formyl)pyrazolylandrosta-5,16-dienes and their derivatives as potent 17α-hydroxylase/C17,20-lyase inhibitors or antiproliferative agents depending on the substitution pattern of the heteroring, Eur. J. Med. Chem. 120 (2016) 284–295, https://doi.org/10.1016/j.ejmech.2016.05.006.
[22] T. Mosmann, Rapid colorimetric assay for cellular growth and survival: application to proliferation and cytotoxicity assays, J. Immunol. Methods 65 (1983) 55–63, https://doi.org/10.1016/0022-1759(83)90303-4.
[23] A. Demjén, R. Alföldi, A. Angyal, M. Gyuris, L. Hackler, G.J. Szebeni, J. Wölfling, L. G. Puskás, I. Kanizsai, Synthesis, cytotoxic characterization, and SAR study of imidazo[1,2- *b*]pyrazole-7-carboxamides, Arch. Pharm. 351 (2018), 1800062, https://doi.org/10.1002/ardp.201800062.
[24] B. Alföldi, H. Faragó, N. Kotogány, F. Nagy, P. Szebeni, Single cell mass cytometry of non-small cell lung cancer cells reveals complexity of in vivo and three-dimensional models over the Petri-dish, Cells 8 (2019) 1093, https://doi.org/10.3390/cells8091093.
[25] E. Kotogány, J.Á. Balog, L.I. Nagy, R. Alföldi, V. Bertagnolo, F. Brugnoli, A. Demjén, A.K. Kovács, P. Batár, G. Mezei, R. Szabó, I. Kanizsai, C. Varga, L. G. Puskás, G.J. Szebeni, Imidazo[1,2-b]pyrazole-7-carboxamide derivative induces differentiation-coupled apoptosis of immature myeloid cells such as acute myeloid leukemia and myeloid-derived suppressor cells, Int. J. Mol. Sci. 21 (2020) 5135, https://doi.org/10.3390/ijms21145135.
[26] J.Á. Balog, L. Hackler Jr., A.K. Kovács, P. Neuperger, R. Alföldi, L.I. Nagy, L. G. Puskás, G.J. Szebeni, Single cell mass cytometry revealed the immunomodulatory effect of cisplatin via downregulation of splenic CD44+, IL-17A+ MDSCs and promotion of circulating IFN-γ+ myeloid cells in the 4T1 metastatic breast cancer model, Int. J. Mol. Sci. 21 (2019) 170, https://doi.org/10.3390/ijms21010170.
[27] A. Gyovai, R. Minorics, A. Kiss, E. Mernyák, G. Schneider, A. Szekeres, E. Kerekes, I. Ocsovszki, I. Zupkó, Antiproliferative properties of newly synthesized 19-nor-testosterone analogs without substantial androgenic activity, Front. Pharmacol. 9 (2018) 825, https://doi.org/10.3389/fphar.2018.00825.
[28] B.A. Pulaski, S. Ostrand-Rosenberg, Mouse 4T1 breast tumor model, Curr. Protoc. Immunol. 39 (2000), https://doi.org/10.1002/0471142735.im2002s39.
[29] B. Schrörs, S. Boegel, C. Albrecht, T. Bukur, V. Bukur, C. Holtsträter, C. Ritzel, K. Manninen, A.D. Tadmor, M. Vormehr, U. Sahin, M. Löwer, Multi-Omics characterization of the 4T1 murine mammary gland tumor model, Front. Oncol. 10 (2020) 1195, https://doi.org/10.3389/fonc.2020.01195.
[30] E.J. Folkerd, M. Dowsett, Influence of sex hormones on cancer progression, J. Clin. Oncol. 28 (2010) 4038–4044, https://doi.org/10.1200/JCO.2009.27.4290.
[31] W. Schönfeld, J. Weiland, C. Lindig, M. Masnyk, M.M. Kabat, A. Kurek, J. Wicha, K. R.H. Repke, The lead structure in cardiac glycosides is 5ß,14ß-androstane-3ß,14-diol, Naunyn-Schmiedeberg Arch. Pharm. 329 (1985) 414–426, https://doi.org/10.1007/BF00496377.
[32] F. Jourdan, C. Bubert, M.P. Leese, A. Smith, E. Ferrandis, S. Regis-Lydi, S. P. Newman, A. Purohit, M.J. Reed, B.V.L. Potter, Effects of C-17 heterocyclic substituents on the anticancer activity of 2-ethylestra-1,3,5(10)-triene-3-O-sulfamates: synthesis, in vitro evaluation and computational modelling, Org. Biomol. Chem. 6 (2008) 4108–4119, https://doi.org/10.1039/b810300c.
[33] Y. Ling, J. Li, Y. Liu, K. Kato, G.T. Klus, A. Brodie, 17-imidazolyl, pyrazolyl, and isoxazolyl androstene derivatives. Novel steroidal inhibitors of human cytochrome $C_{17,20}$-lyase ($P450_{17\alpha}$)†, J. Med. Chem. 40 (1997) 3297–3304, https://doi.org/10.1021/jm970337k.
[34] A.H. Banday, B.P. Mir, I.H. Lone, K.A. Suri, H.M.S. Kumar, Studies on novel D-ring substituted steroidal pyrazolines as potential anticancer agents, Steroids 75 (2010) 805–809, https://doi.org/10.1016/j.steroids.2010.02.014.
[35] H. Escriva, F. Delaunay, V. Laudet, Ligand binding and nuclear receptor evolution, BioEssays News Rev. Mol. Cell. Dev. Biol. 22 (2000) 717–727, https://doi.org/10.1002/1521-1878(200008)22:8<717::AID-BIES5>3.0.CO;2-I.
[36] W. Gao, C.E. Bohl, J.T. Dalton, Chemistry and structural biology of androgen receptor, Chem. Rev. 105 (2005) 3352–3370, https://doi.org/10.1021/cr020456u.
[37] D.S. Jakimov, V.V. Kojić, L.D. Aleksić, G.M. Bogdanović, J.J. Ajduković, E. A. Djurendić, K.M. Penov Gaši, M.N. Sakač, S.S. Jovanović-Šanta, Androstane derivatives induce apoptotic death in MDA-MB-231 breast cancer cells, Bioorg. Med. Chem. 23 (2015) 7189–7198, https://doi.org/10.1016/j.bmc.2015.10.015.
[38] D. Kovács, J. Wölfling, N. Szabó, M. Szécsi, R. Minorics, I. Zupkó, É. Frank, Efficient access to novel androsteno-17-(1′,3′,4′)-oxadiazoles and 17β-(1′,3′,4′)-thiadiazoles via N-substituted hydrazone and N,N′-disubstituted hydrazine intermediates, and their pharmacological evaluation in vitro, Eur. J. Med. Chem. 98 (2015) 13–29, https://doi.org/10.1016/j.ejmech.2015.05.010.
[39] L.L. Romero-Hernández, P. Merino-Montiel, S. Meza-Reyes, J.L. Vega-Baez, Ó. López, J.M. Padrón, S. Montiel-Smith, Synthesis of unprecedented steroidal spiro heterocycles as potential antiproliferative drugs, Eur. J. Med. Chem. 143 (2018) 21–32, https://doi.org/10.1016/j.ejmech.2017.10.063.
[40] J. Li, H. Huo, R. Guo, B. Liu, L. Li, W. Dan, X. Xiao, J. Zhang, B. Shi, Facile and efficient access to Androsten-17-(1′,3′,4′)-pyrazoles and Androst-17β-(1′,3′,4′)-pyrazoles via Vilsmeier reagents, and their antiproliferative activity evaluation in vitro, Eur. J. Med. Chem. 130 (2017) 1–14, https://doi.org/10.1016/j.ejmech.2017.02.033.
[41] H. Dillekås, M.S. Rogers, O. Straume, Are 90% of deaths from cancer caused by metastases? Cancer Med 8 (2019) 5574–5576, https://doi.org/10.1002/cam4.2474.
[42] J.N. Lichterman, R. Post, L. Menken, B. Saad, J. Delgado, L. Sall, M. Karr, Pi Kozlowski, K. Degenhardt, A novel role for 17-B estradiol and testosterone in osteosarcoma tumorigenesis and metastasis, JCO 35 (2017), e23012, https://doi.org/10.1200/JCO.2017.35.15_suppl.e23012.
[43] C. Boni, M. Pagano, M. Panebianco, A. Bologna, N.M.A. Sierra, R. Gnoni, D. Formisano, G. Bisagni, Therapeutic activity of testosterone in metastatic breast cancer, Anticancer Res 34 (2014) 1287–1290.
[44] A. Majumder, M. Singh, S.C. Tyagi, Post-menopausal breast cancer: from estrogen to androgen receptor, Oncotarget 8 (2017) 102739–102758, https://doi.org/10.18632/oncotarget.22156.
[45] P. Giovannelli, M. Di Donato, F. Auricchio, G. Castoria, A. Migliaccio, Androgens induce invasiveness of triple negative breast cancer cells through AR/Src/PI3-K complex assembly, Sci. Rep. 9 (2019) 4490, https://doi.org/10.1038/s41598-019-41016-4.
[46] S.P.H. Chiang, R.M. Cabrera, J.E. Segall, Tumor cell intravasation, Am. J. Physiol. Cell Physiol. 311 (2016) C1–C14, https://doi.org/10.1152/ajpcell.00238.2015.
[47] D.A. Fennell, P. Baas, P. Taylor, A.K. Nowak, D. Gilligan, T. Nakano, J.A. Pachter, D.T. Weaver, A. Scherpereel, N. Pavlakis, J.P. van Meerbeeck, S. Cedrés, L. Nolan, H. Kindler, J.G.J.V. Aerts, Maintenance defactinib versus placebo after first-line chemotherapy in patients with merlin-stratified pleural mesothelioma: COMMAND—a double-blind, randomized, phase II study, J. Clin. Oncol. 37 (2019) 790–798, https://doi.org/10.1200/JCO.2018.79.0543.

[48] D.E. Gerber, D.R. Camidge, D. Morgensztern, J. Cetnar, R.J. Kelly, S. S. Ramalingam, D.R. Spigel, W. Jeong, P.P. Scaglioni, S. Zhang, M. Li, D.T. Weaver, L. Vaikus, M. Keegan, J.C. Horobin, T.F. Burns, Phase 2 study of the focal adhesion kinase inhibitor defactinib (VS-6063) in previously treated advanced KRAS mutant non-small cell lung cancer, Lung Cancer 139 (2020) 60–67, https://doi.org/10.1016/j.lungcan.2019.10.033.

[49] B. Corkery, J. Crown, M. Clynes, N. O'Donovan, Epidermal growth factor receptor as a potential therapeutic target in triple-negative breast cancer, Ann. Oncol. 20 (2009) 862–867, https://doi.org/10.1093/annonc/mdn710.

[50] P. Zhang, Y. Ma, C. Lv, M. Huang, M. Li, B. Dong, X. Liu, G. An, W. Zhang, J. Zhang, L. Zhang, S. Zhang, Y. Yang, Upregulation of programmed cell death ligand 1 promotes resistance response in non-small-cell lung cancer patients treated with neo-adjuvant chemotherapy, Cancer Sci. 107 (2016) 1563–1571, https://doi.org/10.1111/cas.13072.

[51] J. Ni, P. Cozzi, J. Beretov, W. Duan, J. Bucci, P. Graham, Y. Li, Epithelial cell adhesion molecule (EpCAM) is involved in prostate cancer chemotherapy/radiotherapy response in vivo, BMC Cancer 18 (2018) 1092, https://doi.org/10.1186/s12885-018-5010-5.

[52] J. Kim, J. Kim, J.-S. Bae, ROS homeostasis and metabolism: a critical liaison for cancer therapy, Exp. Mol. Med. 48 (2016) 269, https://doi.org/10.1038/emm.2016.119.

[53] D. Whitaker-Menezes, U.E. Martinez-Outschoorn, Z. Lin, A. Ertel, N. Flomenberg, A.K. Witkiewicz, R. Birbe, A. Howell, S. Pavlides, R. Gandara, R.G. Pestell, F. Sotgia, N.J. Philp, M.P. Lisanti, Evidence for a stromal-epithelial "lactate shuttle" in human tumors: MCT4 is a marker of oxidative stress in cancer-associated fibroblasts, Cell Cycle 10 (2011) 1772–1783, https://doi.org/10.4161/cc.10.11.15659.

[54] U.E. Martinez-Outschoorn, R. Balliet, Z. Lin, D. Whitaker-Menezes, R.C. Birbe, A. Bombonati, S. Pavlides, R. Lamb, S. Sneddon, A. Howell, F. Sotgia, M.P. Lisanti, BRCA1 mutations drive oxidative stress and glycolysis in the tumor microenvironment: implications for breast cancer prevention with antioxidant therapies, Cell Cycle 11 (2012) 4402–4413, https://doi.org/10.4161/cc.22776.

[55] F. Baenke, S. Dubuis, C. Brault, B. Weigelt, B. Dankworth, B. Griffiths, M. Jiang, A. Mackay, B. Saunders, B. Spencer-Dene, S. Ros, G. Stamp, J.S. Reis-Filho, M. Howell, N. Zamboni, A. Schulze, Functional screening identifies MCT4 as a key regulator of breast cancer cell metabolism and survival: MCT4 supports breast cancer cell survival, J. Pathol. 237 (2015) 152–165, https://doi.org/10.1002/path.4562.

[56] S. Oh, H. Kim, K. Nam, I. Shin, Silencing of Glut1 induces chemoresistance via modulation of Akt/GSK-3β/β-catenin/survivin signaling pathway in breast cancer cells, Arch. Biochem. Biophys. 636 (2017) 110–122, https://doi.org/10.1016/j.abb.2017.08.009.

[57] L. Cao, H. Chang, X. Shi, C. Peng, Y. He, Keratin mediates the recognition of apoptotic and necrotic cells through dendritic cell receptor DEC205/CD205, Proc. Natl. Acad. Sci. 113 (2016) 13438–13443, https://doi.org/10.1073/pnas.1609331113.

[58] N. Beauchemin, A. Arabzadeh, Carcinoembryonic antigen-related cell adhesion molecules (CEACAMs) in cancer progression and metastasis, Cancer Metastasis Rev. 32 (2013) 643–671, https://doi.org/10.1007/s10555-013-9444-6.

[59] I. Boutas, A. Potiris, W. Brenner, A. Lebrecht, A. Hasenburg, S. Kalantaridou, M. Schmidt, The expression of galectin-3 in breast cancer and its association with chemoresistance: a systematic review of the literature, Arch. Gynecol. Obstet. 300 (2019) 1113–1120, https://doi.org/10.1007/s00404-019-05292-9.

[60] L. Flamant, E. Roegiers, M. Pierre, A. Hayez, C. Sterpin, O. De Backer, T. Arnould, Y. Poumay, C. Michiels, TMEM45A is essential for hypoxia-induced chemoresistance in breast and liver cancer cells, BMC Cancer 12 (2012) 391, https://doi.org/10.1186/1471-2407-12-391.